


## RESEARCH ARTICLE

# Comparative cranial biomechanics reveal that Late Cretaceous tyrannosaurids exerted relatively greater bite force than in early-diverging tyrannosauroids

Evan Johnson-Ransom<sup>1</sup>  | Feng Li<sup>2</sup> | Xing Xu<sup>3,4</sup> | Raul Ramos<sup>5</sup> | Adam J. Midzuk<sup>6</sup> | Ulrike Thon<sup>7</sup> | Kyle Atkins-Weltman<sup>8</sup> | Eric Snively<sup>9</sup>

<sup>1</sup>Department of Organismal Biology and Anatomy, University of Chicago, Chicago, Illinois, USA

<sup>2</sup>Tianjin Natural History Museum, Tianjin, China

<sup>3</sup>Centre for Vertebrate Evolutionary Biology, Yunnan University, Kunming, China

<sup>4</sup>Key Laboratory of Vertebrate Evolution and Human Origins, Institute of Vertebrate Paleontology and Paleoanthropology, Chinese Academy of Sciences, Beijing, China

<sup>5</sup>Illustration Department, Rocky Mountain College of Art and Design, Lakewood, Colorado, USA

<sup>6</sup>Evolutionary Studies Institute, School of Geosciences, University of the Witwatersrand, Johannesburg, South Africa

<sup>7</sup>Informatik Department, Mannheim University of Applied Sciences, Mannheim, Germany

<sup>8</sup>College of Osteopathic Medicine, Oklahoma State University, Tulsa, Oklahoma, USA

<sup>9</sup>Oklahoma State University College of Osteopathic Medicine—Cherokee Nation, Tahlequah, Oklahoma, USA

## Correspondence

Evan Johnson-Ransom, Department of Organismal Biology and Anatomy, University of Chicago, 1027 E. 57th Street, Chicago, IL 60637, USA.

Email: [ejohnsonransom@uchicago.edu](mailto:ejohnsonransom@uchicago.edu)

## Abstract

*Tyrannosaurus* has been an exemplar organism in feeding biomechanical analyses. An adult *Tyrannosaurus* could exert a bone-splintering bite force, through expanded jaw muscles and a robust skull and teeth. While feeding function of adult *Tyrannosaurus* has been thoroughly studied, such analyses have yet to expand to other tyrannosauroids, especially early-diverging tyrannosauroids (*Dilong*, *Proceratosaurus*, and *Yutyranus*). In our analysis, we broadly assessed the cranial and feeding performance of tyrannosauroids at varying body sizes. Our sample size included small (*Proceratosaurus* and *Dilong*), medium-sized (*Teratophoneus*), and large (*Tarbosaurus*, *Daspletosaurus*, *Gorgosaurus*, and *Yutyranus*) tyrannosauroids, and incorporation of tyrannosaurines at different ontogenetic stages (small juvenile *Tarbosaurus*, *Raptorex*, and mid-sized juvenile *Tyrannosaurus*). We used jaw muscle force calculations and finite element analysis to comprehend the cranial performance of our tyrannosauroids. Scaled subtemporal fenestrae areas and calculated jaw muscle forces show that broad-skulled tyrannosaurines (*Tyrannosaurus*, *Daspletosaurus*, juvenile *Tyrannosaurus*, and *Raptorex*) exhibited higher jaw muscle forces than other similarly sized tyrannosauroids (*Gorgosaurus*, *Yutyranus*, and *Proceratosaurus*). The large proceratosaurid *Yutyranus* exhibited lower cranial stress than most adult tyrannosaurids. This suggests that cranial structural adaptations of large tyrannosaurids maintained adequate safety factors at greater bite force, but their robust crania did not notably decrease bone stress. Similarly, juvenile tyrannosaurines experienced greater cranial stress than similarly-sized earlier tyrannosauroids, consistent with greater adductor muscle forces in the juveniles, and with crania no more robust than in their small adult predecessors. As adult tyrannosauroid body size increased, so too did relative jaw muscle forces manifested even in juveniles of giant adults.

## KEYWORDS

biomechanics, Dinosauria feeding, Paleontology, Theropoda

## 1 | INTRODUCTION

Biomechanical analyses have assessed the feeding function and ecological role of dinosaurs, especially theropods (Carpenter, 2002; Erickson & Olson, 1996; Farlow, 1976; Farlow & Holtz, 2002; Gignac et al., 2010; Rayfield, 2004; Sakamoto (2006, 2010). Theropod dinosaurs have been subject to various analyses addressing their feeding function, offering numerous perspectives about the evolution of feeding behavior in theropod clades. Early small-bodied theropods such as *Eodromaeus* and *Coelophysis* were general carnivores in their environments (Martinez et al., 2011). Upon extinction of terrestrial carnivorous pseudosuchians, theropods occupied the vacancy and became the new dominant predators, ranging toward powerful predators such as *Allosaurus* and *Tyrannosaurus* (Ezcurra et al., 2017; Whiteside et al., 2010). Here, we apply comparative biomechanics to the evolution, ontogeny, and ecology of feeding in the Tyrannosauroidae, a longeval and diverse clade of predatory dinosaurs.

Tyrannosauroids were a group of highly specialized theropods more closely related to birds than to some other averostran theropods (*Allosaurus* and *Ceratosaurus*). The clade is one of the most well-studied theropod groups (Brusatte et al., 2010; Brusatte & Carr, 2016). Members of the Tyrannosauroidae were characterized by their fused nasals (Brusatte et al., 2010; Molnar, 1991; Osborn, 1906; Snively et al., 2006), premaxillary teeth that are D-shaped in cross section (Farlow et al., 1991; Rowe & Snively, 2021; Therrien et al., 2021), and in some taxa high agility compared to other large theropods (Coombs, 1978; Holtz, 1994, 1995; Snively et al., 2004, 2019; Snively & Russell, 2002, 2003). New fossil material of early diverging tyrannosauroids have been recently recovered, elucidating the evolution of this theropod clade. Small, early tyrannosauroids such as *Guanlong*, *Dilong*, and *Moros* were hypothesized to be generalized carnivores (Brusatte & Carr, 2016; Xu et al., 2004, 2006; Zanno et al., 2019), coeval with large allosauroids. Upon the extinction of large allosauroids in Laurasia (e.g., *Shaochilong*), the tyrannosauroids occupied the vacant niche and became the dominant large predators of the Northern Hemisphere (Brusatte et al., 2009; Brusatte & Carr, 2016; Zanno & Makovicky, 2013).

The most commonly studied taxon within Tyrannosauroidae has been *Tyrannosaurus rex*, a late Maastrichtian-age predator capable of bone-splintering bite force ranging between 35,000 and 60,000 N (Bates & Falkingham, 2012, 2018; Gignac & Erickson, 2017). Many studies have focused on feeding in *Tyrannosaurus*, including bite force estimates, finite element modeling, and analysis of feeding traces (Bates & Falkingham, 2012; Cost et al., 2019; Erickson &

Olson, 1996; Gignac & Erickson, 2017). Features that allowed *Tyrannosaurus* to engage in powerful feeding functions include its expanded jaw and neck muscles, structural proportions of the skull, fused nasals, and a functionally akinetic cranium (Coombs, 1978; Cost et al., 2019; Farlow et al., 1991; Holtz, 1994, 1995; Molnar, 1991; Snively et al., 2004, 2006; Snively & Russell, 2002, 2003). Other analyses have examined feeding function in other tyrannosauroids such as *Gorgosaurus* and *Tarbosaurus* (Hurum & Sabath, 2003; Therrien et al., 2021), but there have been fewer considerations of feeding function broadly across Tyrannosauroidae, including early tyrannosauroids such as *Dilong*, *Guanlong*, and *Yutyrannus* (Xu et al., 2004, 2006, 2012).

The purpose of this study is to evaluate the feeding function in Tyrannosauroidae through muscle force reconstruction and finite element analysis (FEA). In addition to estimating bite force and cranial stresses in adult tyrannosauroids of differing sizes, we incorporated *Tyrannosaurus* specimens at different ontogenetic stages to address possible functional correlations between similarly sized adult tyrannosauroids and *Tyrannosaurus* ontogeny.

To assess feeding function and infer the feeding ecologies of tyrannosauroids, we applied biomechanical analyses to test specific hypotheses.

## 2 | HYPOTHESES

We compared the level of stress present in the finite element models to test the following hypotheses.

**Hypothesis 1.** We identified tyrannosauroids as gracile-snouted and robust-snouted, based on their cranial morphologies. Gracile-snouted tyrannosauroids possessed long and shallow snouts, with the preorbital (snout) region encompassing 70% of the cranium (Carr, 2020; Foster et al., 2022; Lü et al., 2014). Robust-snouted tyrannosauroid crania were tall, broad, and with robust individual elements (height at antorbital fenestra 25% or greater than cranium length; width across lacrimals 35% of cranium length or greater; postorbital dimension between orbit and infratemporal fenestra greater than 10% of cranium length). Based on expectations for structural mechanics of slender versus robust structures, the crania of gracile-snouted tyrannosauroids (juvenile *Tyrannosaurus* and *Dilong*) will show higher absolute cranial stress in contrast to robust-

snouted tyrannosauroids (adult *Tyrannosaurus*, *Tarbosaurus*, and *Gorgosaurus*).

**Hypothesis 2.** As tyrannosauroid body size increased, the level of cranial stress decreased, which is to be expected because linearly larger structures are exponentially more resistant to forces. We infer skull size as a proxy for body mass as in crocodylians (Gignac & O'Brien, 2016; O'Brien et al., 2019), although negative allometry in tyrannosauroid subclades would contradict this assumption.

**Hypothesis 3.** Given the broad skulls of robust tyrannosaurids (Snively et al., 2006), we expect juvenile tyrannosaurines in our sample (*Tyrannosaurus*, *Tarbosaurus*, and *Raptorex*) to exert greater jaw muscle forces than other similarly sized tyrannosauroids (*Teratophoneus*, *Dilong*, and *Proceratosaurus*).

### 3 | MATERIALS AND METHODS

#### 3.1 | Tyrannosauroid specimens

Tyrannosauroid specimens were selected across a large spectrum of body sizes. This sample includes (from smallest to largest, Table 1) *Proceratosaurus*, *Dilong*, *Raptorex*, early-stage juvenile *Tarbosaurus*, late-stage juvenile *Tyrannosaurus*, *Teratophoneus*, *Yutyrannus*, *Gorgosaurus*, *Daspletosaurus*, adult *Tarbosaurus*, adult *Tyrannosaurus*, and senescent adult *Tyrannosaurus* (Carr, 2020). Given the uncertain taxonomic status of *Raptorex*, we include it to represent a generalized morphological condition of an early-stage juvenile tyrannosaurid (Rowe & Snively, 2021), based on histological analyses (Fowler et al., 2011; Woodward et al., 2020). Both *Raptorex* and the juvenile *Tarbosaurus* exhibit similar morphological features (e.g., large orbit, slender mandibles, gracile crania, and ziphodont dentition) indicative of juvenile status (Carr, 2020).

#### 3.2 | Finite element analysis model creation

Calculating the jaw muscle forces and performing FEA on models of tyrannosauroid crania enabled interpretation of the cranial performance in Tyrannosauroidea, and how cranial morphology of these theropods evolved.

We applied FEA to the 3D models of tyrannosauroid crania. FEA is a powerful tool that models the mechanical response of a complex structure to forces to evaluate

**TABLE 1** Tyrannosaurus and other tyrannosauroid specimens used for finite element analyses.

Specimen name	Specimen number	Cranium length (cm)
<i>Proceratosaurus bradleyi</i>	NHM R 4860	23
<i>Yutyrannus huali</i>	ZCDM V5000	60
<i>Dilong paradoxus</i>	IVPP 14243	22
<i>Gorgosaurus libratus</i>	TCMI 2001.89.1	84
<i>Teratophoneus curriei</i>	BYU 8120	66
<i>Daspletosaurus torosus</i>	NMC (CMN) 8506	102
Juvenile <i>Tarbosaurus bataar</i>	MPC-D 107/7	30
Adult <i>Tarbosaurus bataar</i>	ZPAL MgD-1/4	110
<i>Raptorex kriegsteini</i>	LH PV18	29
Juvenile <i>Tyrannosaurus rex</i>	BMRP 2002.4.1	67
Adult <i>Tyrannosaurus rex</i>	USNM 555000	130
Senescent adult <i>Tyrannosaurus rex</i>	FMNH PR 2081	139

its stress and strain (Bright, 2014; Rayfield, 2007; Rowe & Snively, 2021). The application of FEA to modern animals allows us to assess their mechanical feeding capabilities in the context of feeding behavior, and to use extant models as an analog to the mechanical feeding behavior of extinct animals (Cost et al., 2019; Rayfield, 2007; Tseng, 2013; Tseng & Flynn, 2015). FEA enables us to evaluate and comprehend how the skeletal structures of living and extinct animals functioned and their roles throughout animal groups' evolutionary history (Rayfield, 2007).

To maximize our comparative sample of tyrannosauroids, we obtained model surface data through varying methods, including CT (computerized tomography) and surface scans of articulated casts, and digital model reconstructions based on primary observation and literature. All models were compromised in that they lacked endocranial cavities and internal pneumaticity, which would underestimate stresses in the pertinent regions. The stress results therefore serve as hypotheses subject to further testing and refinement, as with box-modeling methods of Rahman and Lautenschlager (2016), fossil specimen scans that capture internal detail, and sensitivity comparisons of solid models versus those with full internal cavities (Rowe & Rayfield, 2022). Errors are likely to be precise between our models, at least in the endocrania of comparably sized subjects.

To maximize precision between models obtained through different methods, we slightly smoothed intracranial joints between models reconstructed from articulated separate elements (*Daspletosaurus* and *Gorgosaurus*) to better match surfaces in whole-cranium-based digital models and scanned casts.

The cranium model sources for the *Tyrannosaurus* specimens (adult and juvenile) consisted of either high-resolution casts that were CT-scanned or surface scanned to process into a 3D surface mesh (e.g., USNM 555000, BMRP 2002.4.1), or rigorous 3D reconstructions that were modeled after original specimens (FMNH PR 2081). CT scans of the cast of BMRP 2002.4.1 and 1/3 scale sculpture of FMNH PR 2081 were at 0.7 mm resolution, at O'Bleness Memorial Hospital (Athens, Ohio) and Foothills Hospital (Calgary, Alberta). The sculpture of FMNH PR 2081 was corrected for the specimen's taphonomic distortion with reference to other *T. rex* specimens. The scan data were imported into visualization and analysis software, Avizo, for surface refinement and preparation for FEA. With Avizo, we made refinements to the high-resolution surface scanned cranium of an adult *T. rex* (USNM 555000), such as cleaning the surfaces filling in empty gaps to reflect *Tyrannosaurus*' real-life skeletal anatomy. For example, we modeled a maxillary fenestra (a fenestra or hole which pierces the maxilla anterior to the antorbital fenestra), a feature that is present in theropod dinosaurs, through Avizo's "Scan Surface to Volume" feature and its "Segmentation Editor" (Rauhut & Fechner, 2005). "Scan Surface to Volume" converts surfaces into slice data, enabling internal modeling of data from surface scans which may include unprepared, "solid" regions of the original specimen. We resampled the new volume data to replicate a "smooth" CT scan, to about 1 mm voxel size.

Similarly, the surface scanned data of the cranium of *Teratophoneus* was imported into Avizo to refine it for FE (finite element) modeling. The nasal airway and maxillary fenestrae of *Teratophoneus* were hollowed out in Avizo, and the palate was refined and reconstructed after the morphology of *Tyrannosaurus* (FMNH PR 2081).

As with the physically sculpted large *Tyrannosaurus* (FMNH PR 2081), the 3D models of *Tarbosaurus* (adult), *Gorgosaurus*, and *Daspletosaurus* were digitally sculpted based on accessioned specimens. *Yutyranus*, *Tarbosaurus* (juvenile), *Dilong*, and *Proceratosaurus* were digitally sculpted after the holotypes (Table 1). The cranial models of *Dilong* and *Proceratosaurus* were sculpted with Zbrush; both *Tarbosaurus* models, *Yutyranus*, *Daspletosaurus*, and *Gorgosaurus* were digitally generated with the commercial software Blender version 2.92, later upgraded to version 3.0.

The models of *Gorgosaurus* and *Daspletosaurus* were based on individually sculpted bones which were articulated into models of the complete crania. The bones were modeled as symmetrical, for idealized reconstructions within the span of likely individual variation and were based on taphonomically undistorted specimens. These models were combined into continuous surfaces in Meshmixer, and their joints smoothed as described above.

Because the holotype skull of *Yutyranus* was flattened in lateral view, its 3D geometry was partly modeled with reference to the model of *Proceratosaurus*, given that the two tyrannosauroids are phylogenetically classified as proceratosaurids. The holotype of *Proceratosaurus bradleyi* lacks the dorsal portion of its cranium and missing cranial elements (e.g., crest) were modeled after the small proceratosaurid, *Guanlong*; this makes our *Proceratosaurus* model a composite proceratosaurid. The digitally sculpted models of the aforementioned tyrannosauroids were aimed to be accurate as possible, with their reconstructions based on published references and comparisons with later members (*Tyrannosaurus*). Two of us (Xu and Li) described the holotypes and paratypes of *Dilong*, *Yutyranus*, and the proceratosaurid *Guanlong*, and approved the proportions and detail of the reconstructed morphologies. Digital models of *Yutyranus* and *Proceratosaurus* are subject to revision but are the best interpretations at the moment.

From the refined surface models for all taxa, we applied Avizo's "prepare generate tetra grid" before generating a solid tetrahedral mesh. This method created biologically realistic models of the crania, with low-aspect-ratio triangles necessary for minimizing strain artifacts. From the surface mesh, we produced tetrahedral solid meshes of the crania with at least 200,000 nodes and 1 million elements each.

The surface scan of *Raptorex* was incompatible with production of a volumetric mesh, with errors triangle overlap we were unable to resolve with Avizo (even through Scan Surface to Volume) or Blender. We created a model of *Raptorex* for meshless structural mechanics in the commercial software program, Simsolid, which is forgiving of such errors. The method works on geometries without the need for discretization (internal meshing), and retains fine surface detail that often requires simplification, and therefore deviations from geometric accuracy, in traditional FEA of biological structures. The same methods for muscle force estimates, constraints, and material properties were applied to the *Raptorex* analysis as for the traditional FEA of other tyrannosauroids. Details of modeling and solution for the meshless *Raptorex* analysis will be revealed in a future study (Snively et al., 2023).



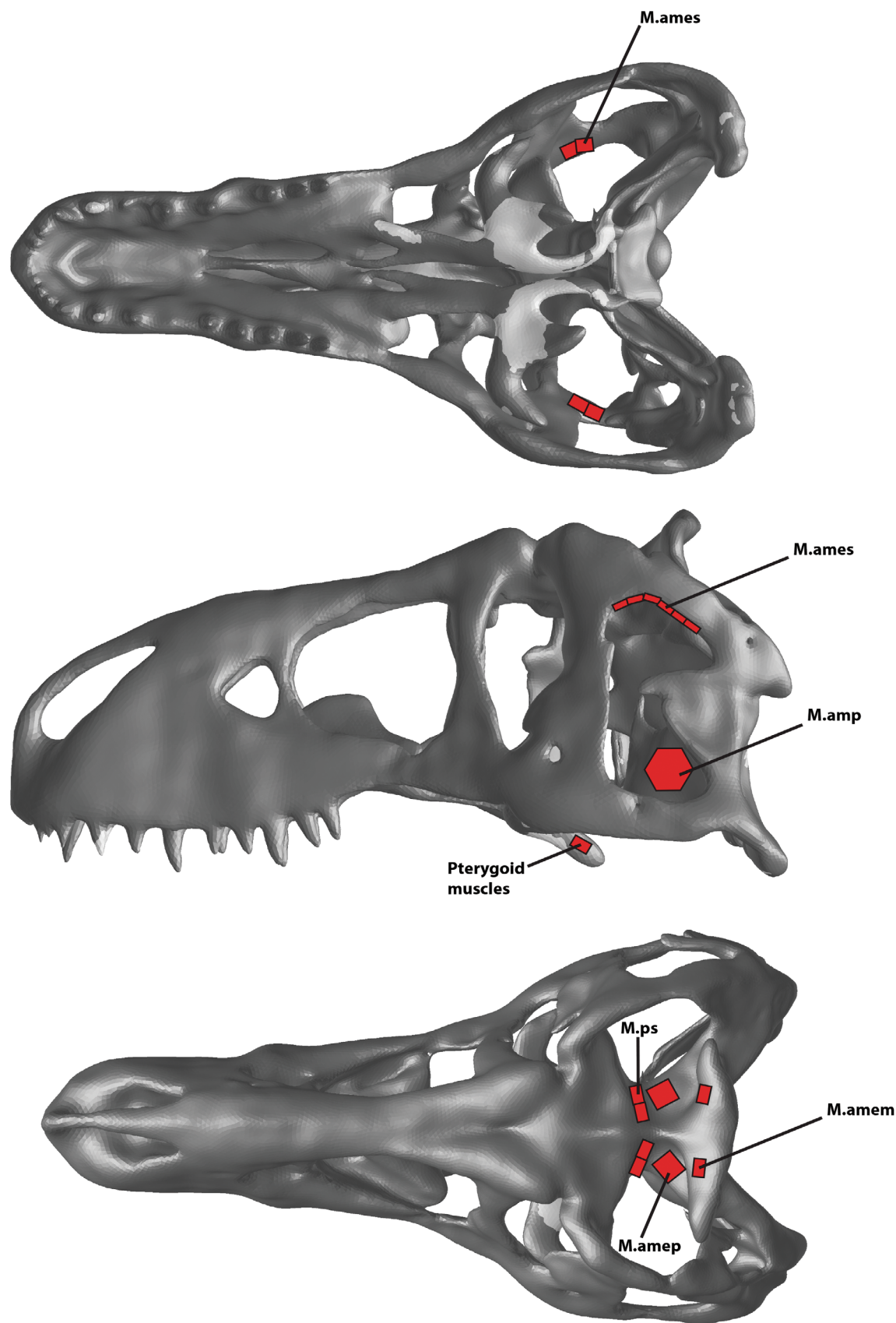


**FIGURE 1** General regions of muscle attachments (Gignac & Erickson, 2017; Holliday, 2009) where forces were applied onto *Tyrannosaurus rex* model in Strand 7. Nodes were sampled on homologous areas of all specimens. Names of the muscles are listed in Table 2.

**TABLE 2** The jaw muscles of tyrannosauroids with their attachments based on inferences of muscle presence (Cost et al., 2019; Gignac & Erickson, 2017; Holliday, 2009; Witmer, 1995).

Abbreviation	Full name	Origin	Insertion
M.ames	M. adductor mandibulae externus superficialis	Medial surface of upper temporal bar	Dorsolateral surface of surangular
M.amem	M. adductor mandibulae externus medialis	Caudolateral portion of temporal fossa	Coronoid eminence/dorsomedial surface of surangular
M.amep	M. adductor mandibulae externus profundus	Caudomedial portion of temporal fossa	Coronoid eminence
M.amp	M. adductor mandibulae posterior	Lateral surface of quadrate	Medial mandibular fossa
M.ps	M. pseudotemporalis complex	Rostromedial portion of temporal fossa	Medial surface of coronoid eminence/rostral medial mandibular fossa
M.int	M. intermandibularis	Anterior half of the splenial	Medial surface of the raphe
M.ptd	M. pterygoideus dorsalis	Dorsal surface of rostral portion of pterygoid and palatine	Medial surface of articular
M.ptv	M. pterygoideus ventralis	Caudovernal surface of pterygoid	Lateral surface of articular and surangular

### 3.3 | Muscle force reconstruction

The muscle forces of the theropod taxa were estimated based on previous muscle reconstructions of archosaurs (Figure 1; Table S2; Gignac & Erickson, 2016, 2017; Holliday, 2009; Lautenschlager, 2013). Identification of muscle origination and insertion were based on osteological correlates (Figure 1; Table 2; Cost et al., 2019; Holliday, 2009; Witmer, 1995). Our reconstruction of the origin of the muscle m. pterygoideus dorsalis was anteriorly restricted following Gignac & Erickson (2017). The muscle likely originated posteriorly from the pterygoid as well (Cost et al., 2019; Holliday, 2009). Differences in stress distributions will be revealing with future analyses comparing the reconstructions. Our estimates of overall force magnitudes converge with those of Cost et al. (2019).

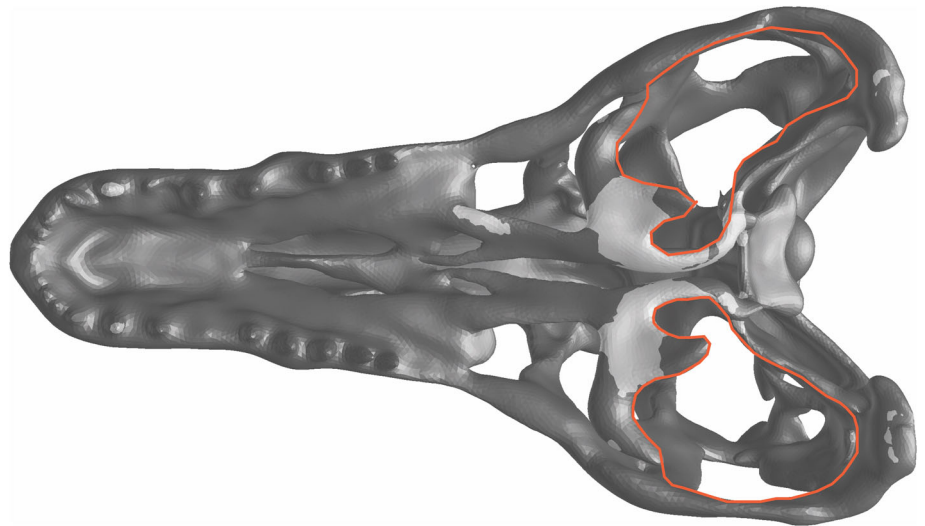
These jaw muscle forces were scaled to those previously estimated for a specimen of *Tyrannosaurus rex* (Gignac & Erickson, 2017; Rowe & Snively, 2021). Specifically, the muscle forces were scaled from the subtemporal fenestrae of the adult *Tyrannosaurus rex* specimen BHI 3033, as jaw muscles penetrate the subtemporal fenestra and insert onto the mandible (Gignac & Erickson, 2017; Rowe & Snively, 2021; Sakamoto, 2010). We used a ratio of areas of the subtemporal fenestrae and multiplied that by the force of BHI 3033 (Gignac & Erickson, 2017; Rowe & Snively, 2021). We applied the same ratio to individual muscles, assuming that individual muscles' areas were scaled the same as the area of the whole subtemporal fenestra.

Although this division of forces enabled consistency between models, it is likely and even certain that the

animals varied in the muscles' relative sizes and contributions to force. For example, the shorter post-temporal bar in *Tarbosaurus* compared with *Tyrannosaurus* suggests a relatively smaller m. adductor mandibulae externus superficialis, which originates from this structure. However, the entire postorbital region of the skull is antero-posteriorly shorter in *Tarbosaurus*, perhaps equalizing the relative forces of individual temporal muscles. Given the escalating permutations, equivalent relative proportions of muscle force is a reasonable baseline assumption, testable with future detailed muscle reconstructions for individual taxa.

We used ImageJ (Schindelin et al., 2012) to directly measure the ventral area of the adductor chamber and calculate the jaw muscle forces (Figure 2). Using figures of tyrannosaur skulls from previous studies, we measured the length of the scale bar in pixels and set the scale in length and units specified in each figure. When measuring the scale bar, the image size was increased, to reduce margins of error. After the scale was set, the tyrannosaur skull was measured, beginning from the posterior end (quadrate) to the anterior or terminal end (premaxilla). This provided the actual length of the theropod's skull. We checked the measurements against those in publications with theropod cranial lengths. Following the measurements, we imported ventral views of the theropods' crania into ImageJ and set the scale based on the recorded measurements of the theropods from lateral view. Our reasoning for using the cranium's ventral view was to reflect the anatomy and direction of the jaw muscles' attachments as the jaw muscles passed through the adductor chamber (Gignac & Erickson, 2017). Using

**FIGURE 2** The jaw muscle forces of the theropods were calculated by measuring the area of subtemporal fenestra of the theropod crania via the measurement software ImageJ. Here, the areas of the subtemporal fenestrae in the *Tyrannosaurus rex* (USNM 555000) are outlined in orange in ventral view.



ImageJ's "polygon tool," we traced the left and right adductor chambers separately.

The physiological cross-sectional area (PCSA) reflected and incorporated the muscle properties of the animal (e.g., volume, length; Zatsiorsky & Prilutsky, 2012). The total muscle force was the sum of both the left and right adductor chambers. To calculate the individual jaw muscle forces of other tyrannosaurs (Equation 1), we used as the baseline the forces from Gignac & Erickson (2017: supporting information) for an adult *Tyrannosaurus* BHI 3033, and scaled force magnitudes for the other tyrannosaurs by ratios of subtemporal fenestra areas, multiplied by an isometric force per area of vertebrate muscle, 31.5 N/cm<sup>2</sup> (Rowe & Snively, 2021)

$$F_{\text{muscle}} = \frac{\text{Area}_{\text{specimen}}}{\text{Area}_{\text{exBHI3033}}} \times F_{\text{muscle}_{\text{exBHI3033}}} \quad (1)$$

This calculation assumes that each respective muscle's anatomical cross-sectional area has the same contribution to total subtemporal fenestra area in all of the tyrannosauroid specimens, and that other contributors to PCSA are constant. The scaling is testable by reconstructing volumes of individual muscles in each specimen, using methods of Gignac & Erickson (2017), Lautenschlager (2013), and Cost et al. (2019). To calculate the muscle force components, we trigonometrically measured the distances and angles of the jaw muscles' origin/insertion, based on our own models and previous studies as seen in Tables S1–S3 (Gignac & Erickson, 2017; Rowe & Snively, 2021). All estimated forces for jaw muscles and total jaw muscle force of the tyrannosauroids are reported in Table 3, and vertical, lateral, and longitudinal muscle force components for each tyrannosauroid specimens are listed in Tables S4–S12.

### 3.4 | Parameters and procedures for FEA

The FE models were imported into Strand7. We applied a Poisson's ratio and elastic moduli as material properties to estimate the object's resistance to elastic deformation and distortion under mechanical loading (Askeland & Phulé, 2006; Greaves et al., 2011). We considered *Alligator* bone as an appropriate model for material properties, because crocodylians are closely related to dinosaurs (Porro et al., 2011). We assumed similar average bone density in the theropods' crania to that of a hard-biting *Alligator*. We therefore assumed similar stiffness and Poisson's ratios to *Alligator's* (Porro et al., 2011) because these properties are proportional to density (Table S13). Lower densities and stiffness, possible in lighter-skulled birds, would result in linearly greater strain but would not greatly affect stresses (Strait et al., 2005) in similarly shaped structures.

We selected nodes in areas of the crania based on reconstructed muscle attachments and the force component magnitudes were divided by the number of nodes to obtain a force per node (Figure 1; Gignac & Erickson, 2017; Holliday, 2009; Lautenschlager, 2013; Rowe & Snively, 2021). We then assigned constraints at the quadrates (the cranial component of the jaw articulation) and at the anterior maxillary teeth, preventing free body motion and simulating a bite at this tooth position.

To compare the stresses and magnitudes displayed by the tyrannosaur skulls, we interpreted von Mises stress that was present in the crania (Rayfield, 2007). In the chosen stress-level color scale, red indicates high stress and blue indicates low stress. A large concentration of red and yellow suggests high regional stress and a large concentration of blue and teal suggest lower stress. We interpret differing stress concentrations as potentially informative about the feeding function of tyrannosauroids.

TABLE 3 Individual and total jaw muscle forces (N) for the tyrannosaurid specimens.

Tyrannosaurid specimens	M. ames	M. amem	M. amep	M. amp	M.ps	M. int	M. ptd	M. ptv	Total jaw muscle force (N)
<i>Proceratosaurus</i> (NHM R 4860)	48	18	44	37	45	26	13	159	390
<i>Yutyrannus</i> (ZCDM V5000)	295	109	269	228	275	163	82	984	2405
<i>Dilong</i> (IVPP 14243)	41	15	38	32	39	23	11	138	337
<i>Gorgosaurus</i> (TCMI 2001.89.1)	1340	496	1224	1034	1248	738	370	4462	10,912
<i>Daspletosaurus</i> (NMC (CMN) 8506)	1763	652	1611	1360	1643	971	487	5873	14,360
<i>Teratophoneus</i> (BYU 8120)	643	237	587	495	599	354	177	2140	5232
<i>Tarbosaurus</i> (MPC-D 107/7)	76	28	70	59	72	42	21	255	623
<i>Tarbosaurus</i> (ZPAL MGD-1/4)	1462	541	1335	1128	1362	805	403	4869	11,905
<i>Raptorex</i> (LH PV18)	142	52	130	109	132	78	39	474	1156
<i>Tyrannosaurus</i> (BMRP 2002.4.1)	1126	416	1028	868	1049	620	310	3750	9167
<i>Tyrannosaurus</i> (USNM 555000)	7942	2958	9124	6449	10,040	3104	1442	19,729	60,788
<i>Tyrannosaurus</i> (FMNH PR 2081)	8273	3082	9504	6718	10,459	3233	1502	20,551	63,322

## 4 | RESULTS

### 4.1 | Ventral areas of the adductor chamber and jaw muscle forces

When comparing the adductor chamber and skull lengths of tyrannosaurids through ontogeny with that of similarly sized tyrannosaurids, the juvenile tyrannosaurines *Tarbosaurus* (juvenile) and *Raptorex* exhibit a greater adductor chamber area (19.76 and 21.28 cm<sup>2</sup>; cranium lengths: 30 and 29 cm) than the small early tyrannosaurids *Dilong* and *Proceratosaurus* (12.36 and 10.71 cm<sup>2</sup>; cranium lengths: 22 and 23 cm). Among medium-sized tyrannosaurids, the juvenile *Tyrannosaurus* (cranium length: 67 cm) has a larger adductor chamber area (200 cm<sup>2</sup>) than the similarly sized *Teratophoneus* (177.41 cm<sup>2</sup>; cranium length: 66 cm). Among large tyrannosaurids, the adult *Tyrannosaurus* has a much larger adductor chamber (992 cm<sup>2</sup>; cranium length: 130 cm) than other large tyrannosaurids such as *Daspletosaurus* (433 cm<sup>2</sup>; cranium length: 102 cm), *Gorgosaurus* (302 cm<sup>2</sup>; cranium length: 84 cm), *Tarbosaurus* (329 cm<sup>2</sup>; cranium length: 110 cm), and *Yutyrannus* (67 cm<sup>2</sup>; cranium length: 60 cm). Adult *Tyrannosaurus* has a wider and longer subtemporal fenestra than in other tyrannosaurids, indicating greater muscle force for its body size (Figure 3) (~30% greater than for a *Daspletosaurus*

cranium scaled to the same length). *Daspletosaurus* exhibits a higher adductor chamber area than *Tarbosaurus* (Figure 3), with a longer but narrower skull.

*Tyrannosaurus* juveniles show expectedly low jaw muscle forces (BMRP 2002.4.1; 9167 N) compared with adults (FMNH PR 2081; 63,322 N) (Figure 4; Table 3). Adult *Tyrannosaurus* such as FMNH PR 2081 and USNM 555000 were capable of exerting high total jaw muscle forces, 63,322 and 60,788 N, respectively, allowing them to apply high tooth forces when biting. Other large robust-snouted tyrannosaurids showed total jaw muscle forces that were lower than that of an adult *Tyrannosaurus* (Figure 4). This included *Tarbosaurus*, *Daspletosaurus*, and *Gorgosaurus* having total jaw muscle forces of 11,905, 14,360, and 10,912 N, respectively; *Daspletosaurus* possessed the highest total jaw muscle force. The total jaw muscle forces of the robust-snouted tyrannosaurids were higher than the total jaw muscle force of a late-stage juvenile *Tyrannosaurus* (9167 N). Medium-sized tyrannosaurines such as *Teratophoneus* showed total jaw muscle force of 5232 N with a correspondingly lower adductor chamber area than a juvenile *Tyrannosaurus*. Early-stage juvenile tyrannosaurines such as *Raptorex* (1156 N) and a juvenile *Tarbosaurus* (623 N) showed high total jaw muscle forces than small, early-diverging tyrannosaurids (*Proceratosaurus*, 390 N and *Dilong* 337 N). Both *Raptorex* and the juvenile *Tarbosaurus*



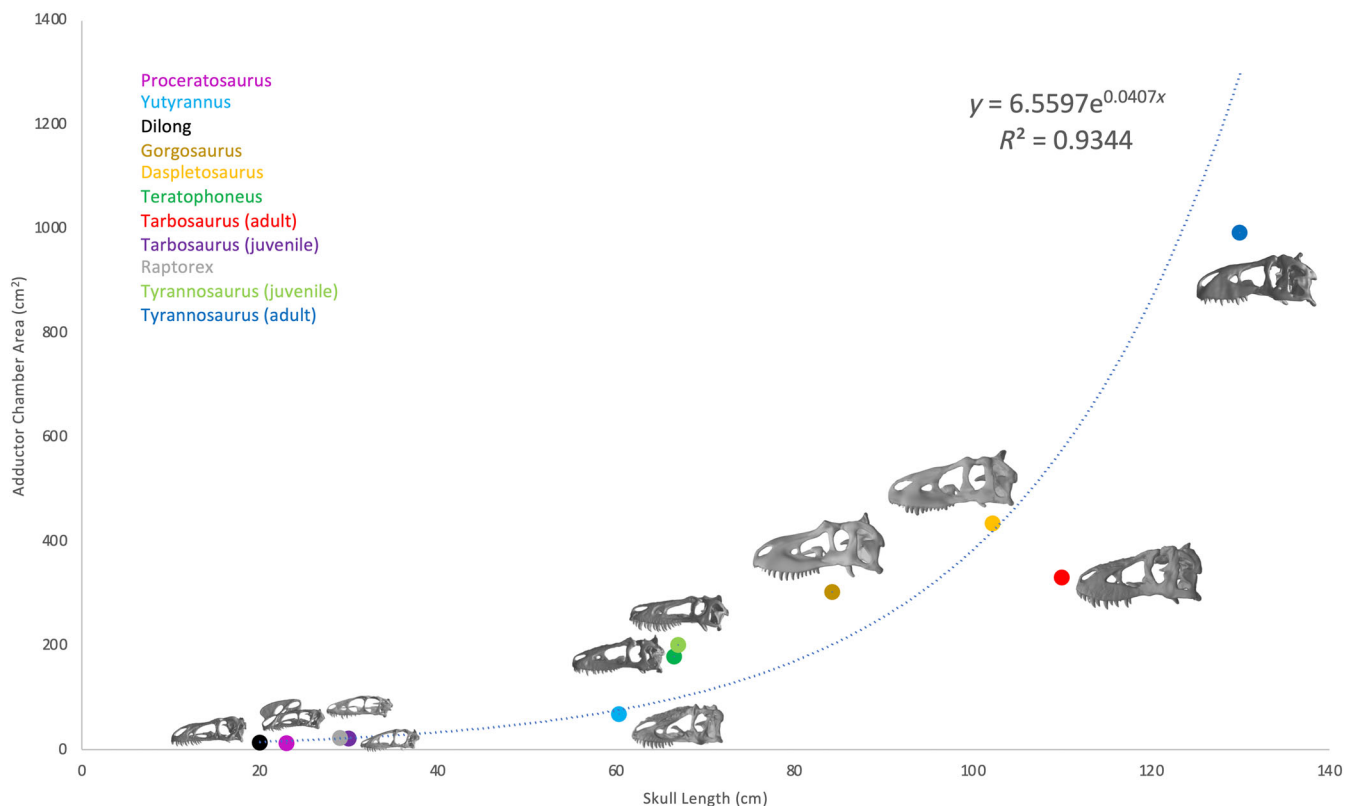


**FIGURE 3** Adductor chamber area regressed against skull length. Juvenile tyrannosaurines such as *Raptorex* and juvenile *Tarbosaurus* and *Tyrannosaurus* exhibit a larger adductor chamber area than similarly sized tyrannosauroids such as *Dilong*, *Proceratosaurus*, and *Teratophoneus*. Adult *Tyrannosaurus* possessed a relatively greater adductor chamber area than other large tyrannosauroids. *Daspletosaurus* has a relatively larger adductor chamber area than the Mongolian tyrannosaurine *Tarbosaurus*, and correspondingly greater bite force for its skull length. Similarly, juvenile *Tyrannosaurus* and *Teratophoneus* have much greater adductor chamber areas than *Yutyranus* at similar skull lengths. Relatively larger adductor chamber area of tyrannosaurids indicate a relatively higher bite force than earlier tyrannosauroids.

possessed a wider adductor chamber than small, early-diverging tyrannosauroids. This would suggest that juvenile tyrannosaurines could exert a higher bite force, a trend that would continue throughout their ontogeny (Figures 5 and 6). The large early-diverging tyrannosauroid *Yutyranus* had a total jaw muscle force of 2405 N, which was lower than a juvenile *Tyrannosaurus* and other large, robust-snouted tyrannosaurids. The large proceratosaurid possessed a skull length (60 cm) that was shorter than that of large, robust-snouted tyrannosaurids (*Tyrannosaurus*, 139 cm; *Daspletosaurus*, 102 cm), but comparable to the skull length of a late-stage juvenile *Tyrannosaurus* (67 cm).

## 4.2 | FEA stresses

Using color-coding of von Mises stresses, we examined the cranial performance of the 3D models and the stress magnitudes present, with red being an indicator for high stress and blue an indicator for low stress. Statistical quantification of such stress differences will be ideal, as with the

pioneering multivariate approaches of Marcé-Nogué et al. (2017). Here, we restrict our interpretation to broad-scale comparisons of stress in homologous cranial regions, because uncertainties in biological input values (muscle morphology and PCSA) recommend cautious global interpretation over subtle, statistically nuanced local variation in stress.

Ontogenetically the level of stress is rather high in the juvenile condition of *Tyrannosaurus* but decreases upon transitioning into the adult condition (Figure 5). Both of the smaller juvenile tyrannosaurines, *Raptorex* and juvenile *Tarbosaurus*, exhibit high cranial stress, although the level of stress magnitude is higher in the former (Figure 6). Both the adult *Tyrannosaurus* and adult *Tarbosaurus* exhibit moderately low cranial stress, although the stress concentrations occur at different locations of the cranium (nasals and lacrimals of *Tyrannosaurus*, and the nasals and maxilla of *Tarbosaurus*; Figure 6).

Although tyrannosauroids (Figure 7) exhibit varying levels of cranial stress, stress concentrations occur at consistent areas of the cranium such as the nasals, lacrimal,

## Muscle Forces of Tyrannosauroids

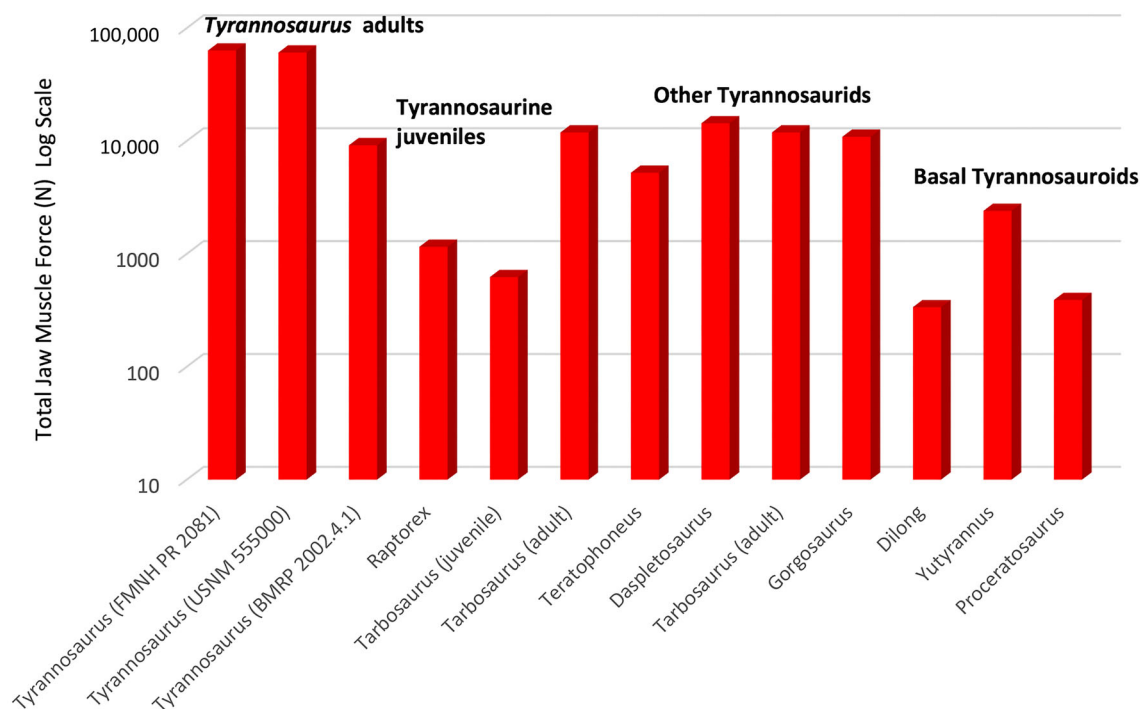


**FIGURE 4** Charted muscle forces of the tyrannosauroid specimens show that adult *Tyrannosaurus* exhibited by far the highest total muscle force. Other adult tyrannosaurids (*Gorgosaurus* and *Daspletosaurus*) show total muscle forces that are either equal to or higher than a late-stage juvenile *Tyrannosaurus*. Small early-diverging tyrannosauroids (*Dilong* and *Proceratosaurus*) exhibit lower muscle forces that are lower than the juvenile tyrannosaurids *Raptorex* and *Tarbosaurus*.

pterygoids, and quadrate. Small, early tyrannosauroids and juvenile tyrannosaurines show higher von Mises stress than the low values present in robust-snouted tyrannosauroids (*Tyrannosaurus*, *Yutyrannus*).

The proceratosaurid *Proceratosaurus* (NHM R 4860) shows primarily low cranial stress in the maxilla, lacrimals, postorbitals, quadrates, quadratojugals, and parietals (Figure 7 and Figure S1). Low stress occurs in the crest of *Proceratosaurus*, along with high stress being present in the palate and pterygoid of *Proceratosaurus*. *Proceratosaurus* is similar in size to *Raptorex* and *Dilong* but shows overall lower cranial stress.

The large proceratosaurid *Yutyrannus* (ZCDM V5000) shows low von Mises stress distributions throughout its cranium such as the maxilla, lacrimals, frontals, and parietals, and quadratojugal (Figure 7 and Figure S2). Similar to other tyrannosauroids, high palatal stress is present in *Yutyrannus*. The rugose nasals of *Yutyrannus* show primarily low stress, similar to the crest of *Proceratosaurus*.

The early pantyrannosaur *Dilong* (IVPP 14243) shows similar cranial stress distributions to the adult *Tyrannosaurus* USNM 555000. Low stress occurs at the nasal-lacrimal suture, lacrimal, parietals, and quadratojugal (Figure 7 and Figure S3). High stress is present at the

palate and pterygoids. The palatal stress of *Dilong* is higher than that in *Proceratosaurus*, but lower than in *Raptorex*.

The albertosaurine *Gorgosaurus* (TCMI 2001.89.1) exhibits stress magnitude distribution analogous to that of *Teratophoneus* (Figure 7 and Figure S4). Relatively lower stress magnitudes are present in the nasals, nasal-lacrimal suture, lacrimal bar, maxilla, quadratojugal, squamosals, and vomer. Moderately low stress does occur at the quadrate and palate. *Gorgosaurus* exhibits lower cranial stresses than the similarly sized tyrannosaurine *Daspletosaurus*. Similar to other large tyrannosaurids, *Gorgosaurus* exhibits high palatal stress in contrast to the lower palatal stress in *Teratophoneus*.

The North American tyrannosaurid, *Daspletosaurus* (NMC [CMN] 8506) exhibits higher stress magnitudes than the similarly sized albertosaurine, *Gorgosaurus* (Figure 7 and Figure S5). Higher stress magnitudes are present in the nasals, nasal-maxillary suture, and the palate. *Daspletosaurus* exhibits higher palatal stress in its pterygoid flanges than *Gorgosaurus*. Low cranial stress magnitudes are present in the squamosal, lacrimal, postorbital, and quadrate.

*Teratophoneus* (BYU 8120), an early robust-snouted tyrannosaurine, exhibits lower stress magnitudes than

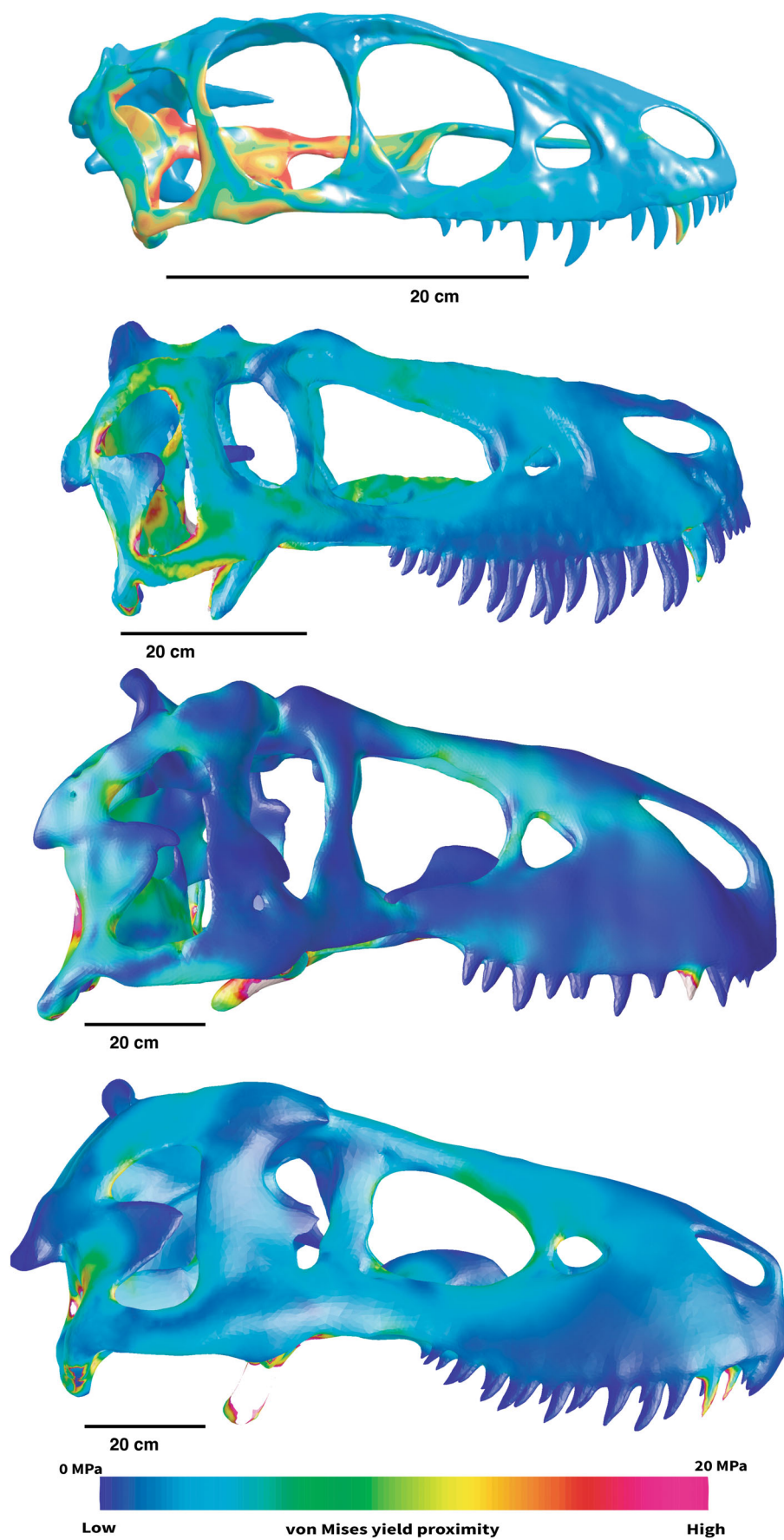
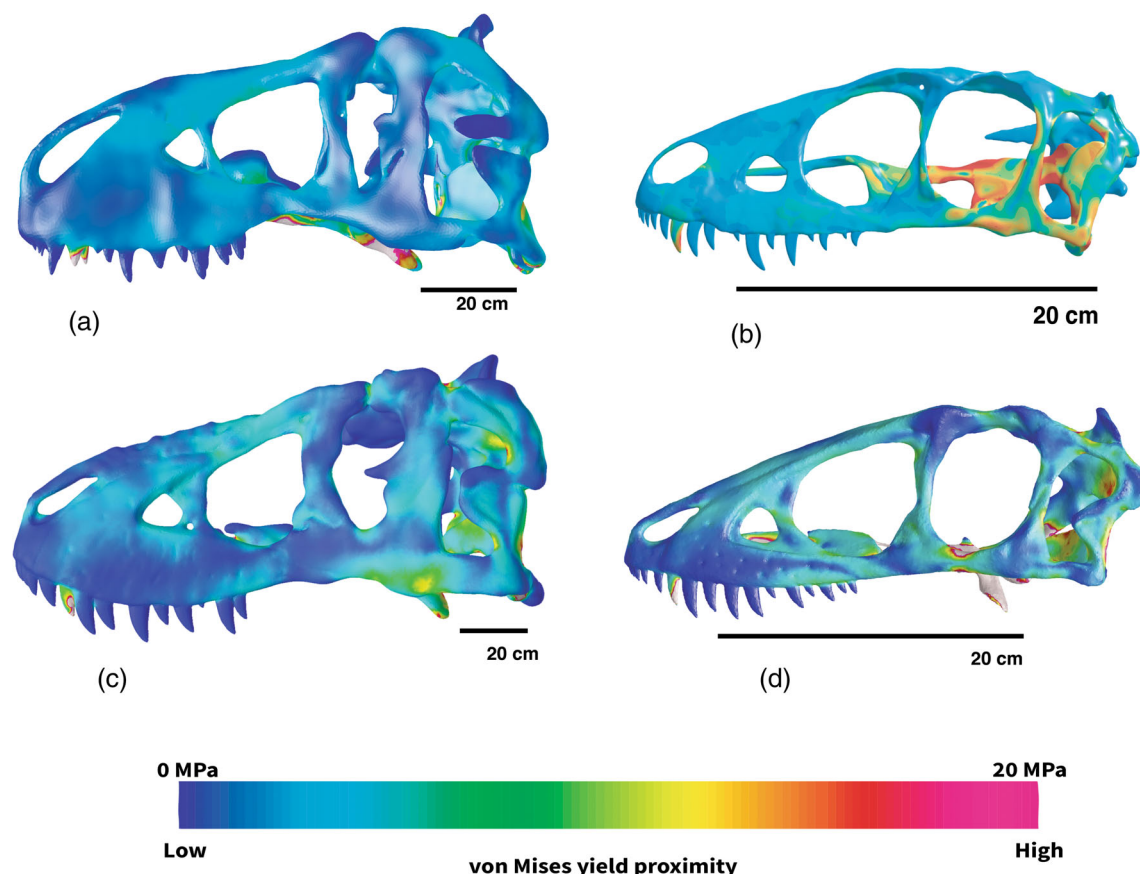


FIGURE 5 Legend on next page.



**FIGURE 6** Ontogenetic comparisons of and adult *Tyrannosaurus* (a), *Raptor* (b), and an adult and juvenile *Tarbosaurus* (c and d, respectively). The adult *Tyrannosaurus* and *Tarbosaurus* display differing stress magnitudes at the jugal and squamosal (see text). *Raptor* displays lower cranial stress in the nasals and maxilla than the juvenile *Tarbosaurus*, although *Raptor* shows higher stress in the palate and postorbital than the juvenile *Tarbosaurus*. The greatest color-visualized stress is 20 MPa; white areas indicate stresses greater than this value. All crania maintained adequate safety factors.

a similarly sized, late-stage juvenile *Tyrannosaurus* (Figure 7 and Figure S6). Lower stress magnitudes are predominantly present in the anterior portion of the cranium (e.g., nasals and maxilla). Moderately low stress occurs at the jugals, squamosals, postorbitals, quadrates, and pterygoid flanges. Low stress magnitudes occur in the palate and pterygoid of *Teratophoneus*.

The juvenile *Tarbosaurus* (MPC-D 107/7) displays stress magnitudes that occur at areas of the cranium similar to those in adult *Tarbosaurus*, although the juvenile condition shows higher cranial stress than the adult

condition (Figure 7 and Figure S7). Moderately low stress is present throughout the nasals, maxillae, lacrimal bars, quadrates, and quadratojugals. Relatively high stress is present in the pterygoid and palate of the juvenile *Tarbosaurus*. The juvenile *Tarbosaurus* shows higher cranial stress than *Raptor* in the nasals and parietal, whereas palatal stress in *Raptor* is higher than the juvenile *Tarbosaurus*. *Raptor* also exhibits a wider adductor chamber than the juvenile *Tarbosaurus*, which contributes to *Raptor*'s high jaw muscle forces.

The Asian tyrannosaurine *Tarbosaurus* (ZPAL MgD-1/4) displays overall lower cranial stress than in other

**FIGURE 5** Comparative von Mises stresses in tyrannosaurine crania, with cooler colors indicating lower proximity to yield (damaging) stress, and hotter colors indicating closer proximity to yield (~80 MPa in shear). Lateral profiles (top to bottom) of *Raptor kriegsteini* (LH PV18), juvenile *Tyrannosaurus* (BMRP 2002.4.1), adult *Tyrannosaurus* (USNM 555000), and senescent adult *Tyrannosaurus* (FMNH PR 2081) crania showing the absolute stress and performance of the *Tyrannosaurus* at various ontogenetic stages. The large adult *Tyrannosaurus* (FMNH PR 2081) has proportionally greater jaw muscle force than the smaller adult yet lacks a relatively taller cranium, and does not have appreciably lower stress despite its greater size. The greatest visualized stress is 20 MPa for all crania; white indicates stress greater than 20 MPa. *Raptor* shows greater palatal stress than in the larger tyrannosaurine specimens.



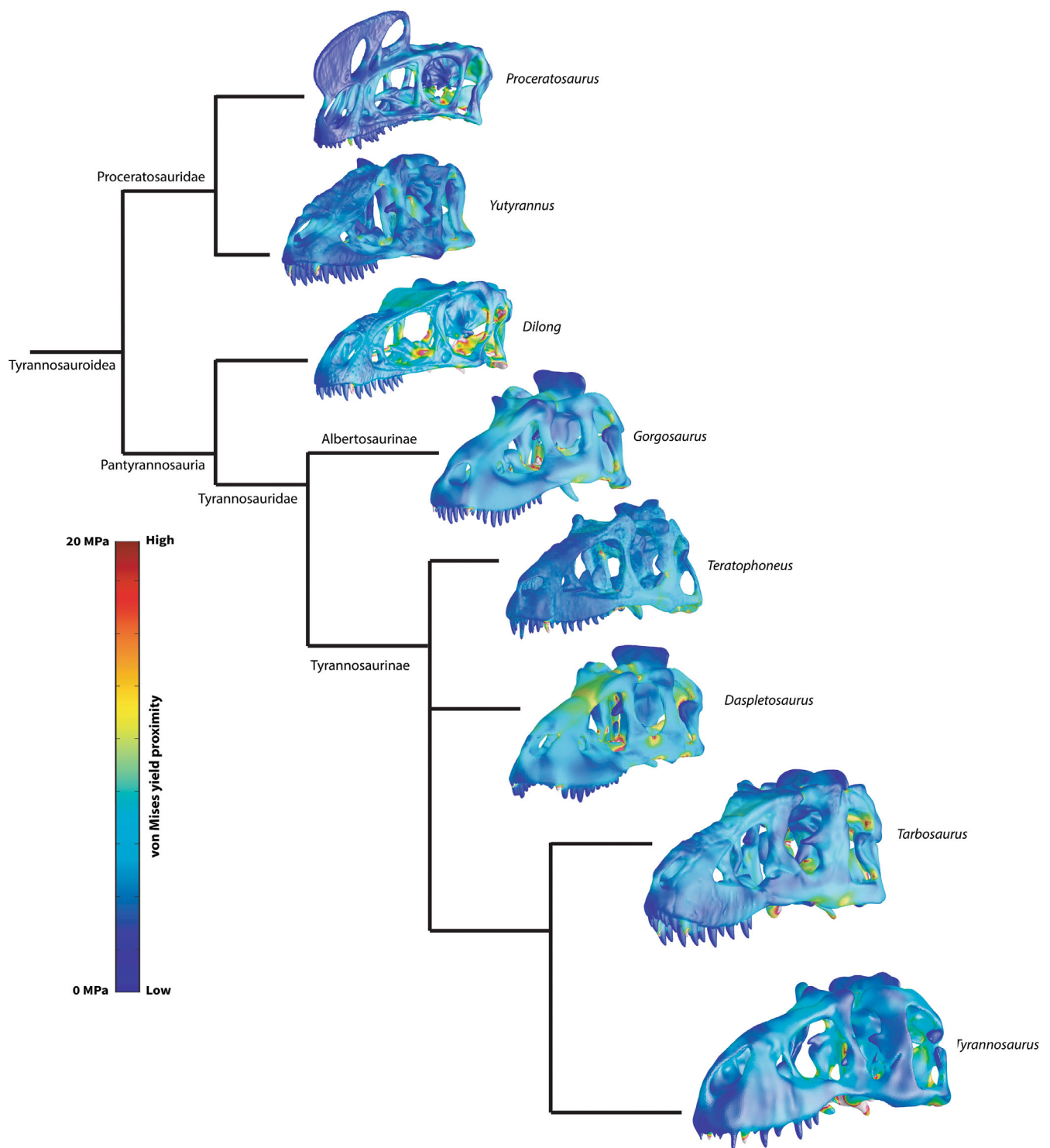


**FIGURE 7** Tyrannosauroids display varying cranial morphologies with differing levels of cranial stress. Greater stresses are typically concentrated in the nasals, lacrimals, quadrate, and postorbitals. Note the cooler colors and lower von Mises stresses in earlier tyrannosauroids, consistent with relatively lower bite forces.

tyrannosaurids, with relatively high stress magnitudes in the palate, the inferior portion of the jugal, the superior portion of the maxilla, and the posterior portion of the quadrate (Figure 7 and Figure S8). In contrast to *Tyrannosaurus* and other North American

tyrannosaurids, stress is prominent in the maxillae, nasals, and maxillary-nasal connection of *Tarbosaurus*. North American tyrannosaurids have stress concentrations occurring at the nasals, lacrimals, and nasal-lacrimal connection.

In *Raptorex* (LH PV18), an early-stage juvenile (Fowler et al., 2011), high cranial stress is present at the lacrimal, postorbital, jugal, quadratojugal, quadrate, and nasal-lacrimal suture (Figure 7 and Figure S9). High stress magnitudes are present in the palate of *Raptorex*. It should be noted that both pterygoideus muscles originate from the palate, with *m. pterygoideus dorsalis* originating at the palatine. High stress occurs at the nasal-lacrimal connection, similar to the juvenile *Tarbosaurus* (Figure 7 and Figure S7).

The juvenile *Tyrannosaurus* (BMRP 2002.4.1) displays lower stress magnitudes than *Raptorex*. Low stress magnitudes are present in the nasals, maxillae, postorbitals, jugals. High peak stress magnitudes are present in the squamosals, quadrates, quadratojugals, and at the pterygoid flanges (Figure 7 and Figure S10). Similar to *Raptorex*, high stress magnitudes are present in the palatine and at the nasal-lacrimal connection of the late-stage juvenile *Tyrannosaurus*.

In an adult *Tyrannosaurus* (USNM 555000), the cranium exhibits stress concentrations similar to other large robust-snouted tyrannosaurids (Figure 7 and Figure S11). Areas of the cranium that show low stress concentrations include the nasals, squamosals, maxillae, quadrates, quadratojugals, and at the nasal-lacrimal suture (Figures 5, 7 and Figure S11). High stress is present at the posterior portion of the quadrate and quadratojugal, as well as at the palatine. High stress occurs at the palatine of the adult *Tyrannosaurus*.

The senescent adult *Tyrannosaurus* (FMNH PR 2081) exhibits stress patterns in regions of the cranium (e.g., squamosals, nasals, and nasal-lacrimal suture) that are consistent with those in the adult *Tyrannosaurus* (USNM 555000) and a late-stage juvenile *Tyrannosaurus* (Figure 5 and Figure S12). High stresses occur at the posterior portion of the quadrate and pterygoid flanges that are also analogous to stresses in the adult *Tyrannosaurus* (USNM 555000) and a late-stage juvenile *Tyrannosaurus*.

## 5 | DISCUSSION

### 5.1 | Hypothesis summaries

With Hypothesis 1, we expected gracile-snouted tyrannosauroids (juvenile tyrannosaurines and small early tyrannosauroids) to show higher cranial stress than robust-snouted tyrannosauroids. The von Mises results of our tyrannosauroid crania appear to support Hypothesis 1. Juvenile tyrannosaurines (*Raptorex* and juvenile *Tarbosaurus*) show higher cranial stress than small early tyrannosauroids such as *Dilong* and *Proceratosaurus*. Levels of muscle force relative to skull size, including

relatively greater forces in tyrannosaurids than in earlier tyrannosaurines (see Hypothesis 3 discussion) governed stresses more than snout shape and robustness. This implies that there is not an absolute correlation with cranial morphology and cranial performance (von Mises stress), as predicted with Hypothesis 1.

With Hypothesis 2, we expected the level of cranial stress to decrease as tyrannosauroid body size increased. This did not consistently occur. Small tyrannosauroids such as *Proceratosaurus* showed low cranial stress, in contrast to the high cranial stress magnitudes in larger tyrannosauroids (*Gorgosaurus*, juvenile and most adult tyrannosaurines). Adult *Tarbosaurus* and *Teratophoneus* exhibited lower stress magnitudes than other similarly sized tyrannosaurines. Stresses did decrease as expected from juvenile to adult *Tarbosaurus*. These results largely contradict Hypothesis 2.

For Hypothesis 3, we predicted juvenile tyrannosaurines (*Raptorex*, and juvenile *Tarbosaurus*, and *Tyrannosaurus*) would exert higher jaw muscle forces than similarly sized tyrannosauroids (*Dilong*, *Proceratosaurus*, and *Teratophoneus*), given the wide adductor chamber of juvenile tyrannosaurines versus the narrow adductor chamber area of other tyrannosauroids. When scaled proportionally, the calculated jaw muscle forces of juvenile tyrannosaurines were higher than similarly sized tyrannosauroids. Juvenile tyrannosaurines also exhibit higher von Mises stresses than similarly sized tyrannosauroids; *Dilong* and *Teratophoneus* showing lower cranial stress than *Raptorex* and juvenile *Tyrannosaurus*. The enlarged adductor chamber area and high jaw muscle forces indicate that juvenile tyrannosaurines could exert a higher bite force at the teeth (and experienced concomitantly greater cranial stress) than similarly sized tyrannosauroids, consistent with Hypothesis 3.

### 5.2 | Comparative feeding function of similarly-sized tyrannosauroids and *Tyrannosaurus rex*: correspondences are not exact

Ontogenetically the skull of *Tyrannosaurus* transitioned from a gracile-snouted juvenile to a robust-snouted, robust adult. Further analyses have evaluated the dramatic metamorphosis of *Tyrannosaurus* skull morphology including the theropod's skull roof, snout, and mandible (Bates & Falkingham, 2012; Carr, 2020; Rowe & Snively, 2021). The cranium of *Tyrannosaurus* experienced more changes than the mandible (Carr, 2020). The mandibular ramus experienced an increase in height, along with an expansion of the angular, surangular, and dentary (Carr, 2020; Monteiro &

Soares, 1997; Rowe & Snively, 2021). The cranium of juvenile *Tyrannosaurus* was low relative to its length, while the adult condition possessed a relatively taller cranium with inflated cranial protuberances such as expanded lacrimal crests, post-orbitals, and prominent nasal bumps (Carr, 2020). The palatal bones that serve as attachment points of the m. pterygoideus ventralis in an adult *Tyrannosaurus* show significant enhancement, supporting the forcefulness of the adductor jaw musculature (Carr, 2020; Cost et al., 2019; Gignac & Erickson, 2017; Rowe & Snively, 2021).

Because FEA reveals the consequences of dramatic changes in the skull morphology and jaw muscle performance in *Tyrannosaurus*, this study in parallel highlights the correlations and contrasts in the feeding function of similarly sized tyrannosauroids and *Tyrannosaurus* (juvenile *Tyrannosaurus* and *Teratophoneus*; adult *Tyrannosaurus* and *Tarbosaurus*).

Small tyrannosauroids such as *Raptorex*, juvenile *Tarbosaurus*, *Dilong*, and *Proceratosaurus* show cranial stress concentrations in similar areas of the crania such as the quadrate, quadratejugal, parietals, and squamosals. The juvenile tyrannosaurines display higher cranial and palatal stress than *Dilong* and *Proceratosaurus*, a consequence of the juveniles' wider adductor chamber and higher jaw muscle force (especially in *Raptorex*). This suggests that tyrannosaurines as early-stage juveniles, especially *Tyrannosaurus*, were possibly adapted at exerting relatively great muscular forces which would continue throughout its ontogeny (Peterson et al., 2021; Peterson & Daus, 2019; Rowe & Snively, 2021). Similar stress magnitudes in larger *Tyrannosaurus* specimens maintained similar safety factors, despite relatively escalated bite forces.

The late-stage juvenile *Tyrannosaurus*, BMRP 2002.4.1 exhibits higher cranial stress than *Teratophoneus*, a robust-snouted tyrannosaurine. *Teratophoneus* shows lower cranial stress, because the late-stage juvenile *Tyrannosaurus* exhibits a higher bite force than *Teratophoneus*, similarly to *Raptorex* versus other small tyrannosauroids. The adductor chamber of BMRP 2002.4.1 is wider than *Teratophoneus*. This enabled *Tyrannosaurus* juveniles to exert relatively higher bite force than *Teratophoneus*. Although they perforated bone, juvenile *Tyrannosaurus* lacked the ability to splinter bone as seen in the adult condition (Gignac & Erickson, 2017; Peterson et al., 2021; Peterson & Daus, 2019).

Larger tyrannosauroids including an adult *Tyrannosaurus* (FMNH PR 2081 and USNM 555000) exhibit high jaw muscle forces and relatively low cranial stress magnitudes in the nasals and squamosals, although high stress does occur at the palate. Like adult *Tyrannosaurus*, *Daspletosaurus* and *Gorgosaurus* exhibited higher stress and jaw muscle force than adult *Tarbosaurus* and *Yutyrannus*.

Having a deeply robust cranium and an expanded mandible allowed robust-snouted tyrannosauroids such as an adult *Tyrannosaurus*, *Tarbosaurus*, *Daspletosaurus*, and *Gorgosaurus* to resist high forces and deliver powerful bite forces to similarly sized prey (Gignac & Erickson, 2017; Hurum & Sabath, 2003; Rowe & Snively, 2021; Snively et al., 2006; Therrien et al., 2005, 2021).

The FEA results and muscle force analyses support analogous stress magnitudes between similarly sized tyrannosauroids and different aged individuals of *Tyrannosaurus*. The jaw muscle forces, however, suggest that *Tyrannosaurus* at different ontogenetic stages was capable at exhibiting higher bite forces than other similarly sized tyrannosauroids.

### 5.3 | Inferred feeding behavior and paleoecology of early-diverging Tyrannosauroids (*Dilong* and *Proceratosaurids*)

The early-diverging pantyrannosaur *Dilong* (Brusatte & Carr, 2016) shows low cranial stress and a low jaw muscle force in contrast to juvenile tyrannosaurines. This suggests that the diet of *Dilong* may have consisted of smaller prey such as mammals, reptiles, and small maniraptoriformes (Chang et al., 2017). Analyses on the braincase and inner ear of *Dilong* show that the small pantyrannosaur possessed good agility and balance but lacked heightened sense of smell of larger tyrannosauroids (*Bistahieversor* and *Tyrannosaurus*) (Kundrát et al., 2018; McKeown et al., 2020). The fusion of nasals in *Dilong* suggest that they may have been capable of reducing stress when biting, an attribute which would become more pronounced in later tyrannosauroids (Rauhut et al., 2010; Rayfield, 2004; Snively et al., 2006; Xu et al., 2004).

Similarly, to *Dilong*, the small proceratosaurid *Proceratosaurus* displays low cranial stress. Similar to juvenile tyrannosauroids, the teeth of *Proceratosaurus* were ziphodont or flattened, and the animal possessed a relatively slender craniomandibular morphology (Rauhut et al., 2010). This suggests that *Proceratosaurus* and other small proceratosaurids (*Guanlong*) likely fed on smaller prey. Moderate stress was present in the posterior portion of the cranial crest of *Proceratosaurus*, indicating that cranial crests may have acted as a stress sink and buttress while biting, in addition to the crests serving as display features (Rauhut et al., 2010). Fused nasals are also present in proceratosaurids. It has been hypothesized that proceratosaurids (*Proceratosaurus*) and other early tyrannosauroids (*Dilong*) may have employed puncture-pull style feeding (Erickson & Olson, 1996; Rauhut et al., 2010; Rayfield, 2004), and this can be further tested (Snively &

Russell, 2007). The craniomandibular morphology in small proceratosaurids indicate that early tyrannosauroids possessed specialized cranial and dental adaptations unique among theropods (Rauhut et al., 2010).

Large proceratosaurids such as *Yutyrannus* possessed a deeper skull and lacked the large, elaborate cranial crests in contrast to small proceratosaurids (*Guanlong*) (Rauhut et al., 2010; Xu et al., 2006, 2012). Similar to the reconstructed nasals of *Proceratosaurus*, the nasals of *Yutyrannus* exhibited low stress, and may support that the crests of *Yutyrannus* would have been capable of resisting high forces, especially with larger prey. Specimens of *Yutyrannus* at different growth stages (juveniles and adults) were recovered (Xu et al., 2012). *Yutyrannus* may have exhibited niche partitioning with juveniles pursuing smaller prey (*Psittacosaurus* and maniraptoriformes) and adults feeding on larger prey (*Dongbeititan*) (Therrien et al., 2021; Xing et al., 2012; Zhou, 2006). Sauropod material was recovered in the quarry where the *Yutyrannus* specimens were found, suggesting that sauropods were a potential food source for the large proceratosaurid (Xing et al., 2012; Xu et al., 2012).

#### 5.4 | Inferred feeding behavior and paleoecology of Albertosaurines

Recent analyses have examined the feeding behavior, ontogeny, and behavioral ecology of albertosaurines (*Gorgosaurus* and *Albertosaurus*) (Therrien et al., 2021; Voris et al., 2022). Albertosaurines underwent ontogenetic niche partitioning, because the craniomandibular morphology of juveniles differed greatly from that of adults. Juvenile albertosaurines (*Gorgosaurus*) possessed relatively slender jaws with ziphodont tooth morphology, and slender hindlimbs suggesting that juveniles hunted smaller prey (small ornithischians and small theropods) (Therrien et al., 2021). Upon reaching the late juvenile stage, albertosaurines may have started feeding upon larger prey similarly to a juvenile *Tyrannosaurus* (Holtz, 2021; Peterson et al., 2021; Peterson & Daus, 2019; Schroeder et al., 2021; Therrien et al., 2021). As adults, albertosaurines possessed incassate teeth and more robust skulls that were capable of resisting high forces enabling them to feed on large megaherbivores (hadrosaurids and ceratopsians; Therrien et al., 2021).

#### 5.5 | Inferred feeding behavior and paleoecology of other Tyrannosaurines

*Daspletosaurus* shared its environment with a variety of ornithischian dinosaurs and the large albertosaurine

*Gorgosaurus* (Eberth, 1997; Farlow & Pianka, 2002; Russell, 1970). The two tyrannosaurids have been hypothesized as having separate niches in which *Gorgosaurus* fed on more gracile prey (hadrosaurids) and *Daspletosaurus* fed on ceratopsians (Farlow & Pianka, 2002; Russell, 1970). Hadrosaur bones also were recovered in the stomach area of *Daspletosaurus*, suggesting that the tyrannosaurine did not have a specific prey preference (Varricchio, 2001). The two tyrannosaurids appear to have had differing postcranial builds with *Gorgosaurus* being more lightly built and *Daspletosaurus* being more robust, consistent with *Daspletosaurus* having a broader muzzle and *Gorgosaurus* having a lower snout (Snively et al., 2006).

While there have not been recorded feeding traces of the early tyrannosaurine *Teratophoneus*, it can be inferred that *Teratophoneus* would have fed upon similarly sized hadrosaurids and ceratopsids similarly to *Tyrannosaurus* and *Gorgosaurus*, and experienced ontogenetic niche partitioning (Holtz, 2021; Therrien et al., 2021; Zanno & Sampson, 2005). *Teratophoneus* was the only large terrestrial predator of its environment. Bonebeds of *Teratophoneus* specimens at different ages support the possibility of gregarious behavior in tyrannosaurids such as *Albertosaurus* and *Daspletosaurus* (Titus et al., 2021).

Similar to *Tyrannosaurus*, there have been recovered specimens of *Tarbosaurus* at different ontogenetic stages (Tsuihiji et al., 2011). The inferred feeding behavior and ecology of *Tarbosaurus* bears some similarities to that of *Tyrannosaurus*. *Tarbosaurus* shared its environment with large hadrosaurids, titanosaurs, ankylosaurs, and large herbivorous maniraptoriforms, while *Tyrannosaurus* fed on large hadrosaurids and ceratopsians (Bell et al., 2013; Hurum & Sabath, 2003; Maleev, 1955, 1974; Owocki et al., 2019). FEA results for *Tarbosaurus* reveal stress concentrated in the maxilla and lacrimal, corroborating hypotheses of Hurum and Sabath (2003), whereas *Tyrannosaurus* had cranial stress concentrations in the nasals, nasal-lacrimal connection, and lacrimals (Hurum & Sabath, 2003; Rayfield, 2004).

The consequences of these differences are unclear and remain to be tested. Differing stress distributions may reflect that the two large tyrannosaurines fed on different prey. Bite marks attributed to *Tarbosaurus* have been recovered on the bones of hadrosaurids, titanosaurs, and the large ornithomimosaur *Deinocheirus* (Bell et al., 2013; Hurum & Sabath, 2003; Owocki et al., 2019). Although *Tarbosaurus* likely experienced ontogenetic niche partitioning through growth, high bite force in the juveniles suggests the capability for engaging more robust or resistant prey than likely in similarly sized early tyrannosauroid adults (Holtz, 2021; Maleev, 1955, 1974; Therrien et al., 2021).



## 5.6 | Inferred feeding behavior and paleoecology of *Tyrannosaurus*

The results present a profile of *Tyrannosaurus* ontogeny, transitioning from small, generalized carnivores to large-bodied predators. Given their small and gracile skull, juvenile *Tyrannosaurus* were likely incapable of delivering bite forces as great as those of an adult *Tyrannosaurus* when scaled to the same size.

The FEA results for *Raptorex* suggest that an early-stage juvenile tyrannosaurine such as *Tyrannosaurus* would have hunted smaller prey animals, similar to other small-bodied tyrannosauroids (*Dilong* and *Proceratosaurus*). Late-stage juvenile *Tyrannosaurus* likely filled the role of medium-sized predators in “tyrannosaur-rich” environments in contrast to “non-tyrannosaur” environments (Holtz, 2021; Schroeder et al., 2021). A late-stage juvenile *Tyrannosaurus* was more agile than an adult and likely capable of hunting more gracile prey such as ornithomimosaurs, pachycephalosaurs, thescelosaurus, and relatively smaller hadrosaurs and ceratopsians (Currie, 1983; Currie & Eberth, 2010; Dececchi et al., 2020; Erickson et al., 2004; Hutchinson et al., 2011; McCrea et al., 2014; Persons & Currie, 2014; Snively et al., 2019). However, juvenile *Tyrannosaurus* fed upon larger-bodied prey animals such as hadrosaurs but lacked the osteophagous capability of adults (Peterson et al., 2021; Peterson & Daus, 2019).

Given their size and reinforced skull morphology, the larger adult *Tyrannosaurus* served as the apex predators of their environment. Adult *Tyrannosaurus* preyed upon a variety of herbivorous dinosaurs such as ceratopsians and hadrosaurs, with healed bite marks attributed to adult tyrannosaurids along with dinosaur bones being recovered in tyrannosaurid coprolites (fossil feces) (Carpenter, 1997; Chin et al., 1998; DePalma et al., 2013; Happ, 2008; Rothschild & DePalma, 2013; Varricchio, 2001). Stress results are consistent in *Tyrannosaurus* with cranial features such as fused nasals, immobile cranial joints, and robust cranial proportions that allowed tyrannosauroids to resist high compressive forces and display low shear stress. Features such as these enabled *Tyrannosaurus* to engage in predation involving extensive tooth-bone contact, and effective osteophagy in *Tyrannosaurus* (Gignac & Erickson, 2017).

## 6 | CONCLUSION AND FUTURE DIRECTIONS

The presented results are consistent with adaptations in tyrannosauroids such as fused nasals, cranial crests, kinetic cranial joints, a secondary palate, and expanded

adductor chambers that allowed them to deliver powerful bite forces and resist high loadings when feeding (Brusatte et al., 2010; Brusatte & Carr, 2016; Coombs, 1978; Farlow et al., 1991; Holtz, 1994, 1995; Molnar, 1991; Osborn, 1906; Rowe & Snively, 2021; Snively et al., 2004, 2006, 2019; Snively & Russell, 2002, 2003; Therrien et al., 2021). This study focused on broadly assessing the evolution of feeding function in Tyrannosauroida, especially with an emphasis of early diverging tyrannosauroids and other large tyrannosauroids. Early tyrannosauroids such as *Proceratosaurus* and *Dilong* show low cranial stress, suggesting a lower bite force. This serves as a major contrast to the cranial performance of later-diverging juvenile tyrannosaurines (*Raptorex* and juvenile *Tarbosaurus*) which exhibited a higher bite force and higher cranial stress.

The cranial morphologies of tyrannosauroids suggest different feeding adaptations, such as robust-snouted crania adapted for feeding on large prey and gracile-snouted crania adapted for smaller prey (Rowe & Snively, 2021). The current findings offer perspective into further evaluating the feeding function of alioramins, such as *Qianzhousaurus* and *Alioramus*. These tyrannosauroids had longirostrine skulls and gracile hindlimbs. It has been hypothesized that alioramins lacked a powerful bite force and were unable to engage in “puncture pull” style feeding compared to robust-snouted tyrannosaurids (Foster et al., 2022; Rayfield, 2004, 2005a, 2005b). Alioramins have a relatively short and narrow postorbital region suggesting lower jaw muscle forces. They also possessed a notably gracile dentary (Foster et al., 2022) suggesting reduced capacity to absorb high bite forces compared with a more robust dentary in other tyrannosaurids with similar skull lengths (Rowe & Snively, 2021).

There are currently two accessioned alioramin specimens, *Qianzhousaurus sinensis* (GM F10004) and *Alioramus altai* (IGM 100/1844) (Brusatte et al., 2012; Lü et al., 2014). Other *Alioramus* specimens are in the process of being repatriated to Mongolia (Browne & Dashdorj, 2022; Brusatte et al., 2012). Their longirostrine cranial morphologies warrant a future FEA study, to evaluate their comparative feeding ecology.

This study promises fruitful replication of mechanical feeding analyses in other under-studied theropod clades, such as Allosauroida, Spinosauridae, and Abelisauridae. The inclusion of non-tyrannosauroid theropods will facilitate a detailed comparative analysis of tyrannosauroid biology and evolution with other theropods.

## AUTHOR CONTRIBUTIONS

**Evan Johnson-Ransom:** Conceptualization; investigation; writing – original draft; methodology;

writing – review and editing; visualization. **Feng Li:** Writing – review and editing; investigation. **Xing Xu:** Investigation; writing – review and editing. **Raul Ramos:** Visualization; methodology. **Adam J. Midzuk:** Methodology; visualization. **Ulrike Thon:** Methodology; visualization. **Kyle Atkins-Weltman:** Writing – review and editing. **Eric Snively:** Conceptualization; investigation; writing – original draft; writing – review and editing; visualization; supervision.

## ACKNOWLEDGMENTS

David Silva of “Beasts of the Mesozoic” provided the 3D skull models of *Proceratosaurus* NHM R 4860 and *Dilong* IVPP 14243. We acknowledge the CT-scan data provided by Brian Cooley, Prathiba Bali, and Steven Rowe for sculpting, scanning, and making an FE model of the adult *Tyrannosaurus* “Sue” FMNH PR 2081. We thank Dr. Lawrence Witmer, Heather Rockfield, and Ryan Ridgely for scanning and providing surface models of the juvenile *Tyrannosaurus* “Jane” BMRP 2002.4.1. Additional thanks to Jeff Parker for scanning *Raptorex kriegsteini* LH PV18, Gaston Design for providing the surface scans of *Teratophoneus curriei*, and the National Museum of Natural History for providing the surface scans of the adult *Tyrannosaurus* “The Nation’s *T. rex*” USNM 555000. We greatly thank the reviewers, Drs. Stephan Lautenschlager and Ali Nabavizadeh, for their feedback on the manuscript.

## DATA AVAILABILITY STATEMENT

All finite element models are available at this link: <https://bit.ly/3QHgApq>.

## ORCID

Evan Johnson-Ransom  <https://orcid.org/0000-0003-4367-5107>

## REFERENCES

- Askeland, D. R., & Phulé, P. P. (2006). *The science and engineering of materials* (5th ed., p. 198). Cengage Learning.
- Bates, K., & Falkingham, P. (2018). The importance of muscle architecture in biomechanical reconstructions of extinct animals: A case study using *Tyrannosaurus rex*. *Journal of Anatomy*, 233, 625–635.
- Bates, K., & Falkingham, P. L. (2012). Estimating maximum bite performance in *Tyrannosaurus rex* using multi-body dynamics. *Biology Letters*, 8, 660–664.
- Bell, P., Currie, P. J., & Lee, Y.-N. (2013). Tyrannosaur feeding traces on *Deinocheirus* (Theropoda: ?Ornithomimosauria) remains from the Nemegt formation (Late Cretaceous), Mongolia. *Cretaceous Research*, 37, 186–190.
- Bright, J. A. (2014). A review of paleontological finite element models and their validity. *Journal of Paleontology*, 88, 760–769.
- Browne, K. V., & Dashdorj, T. (2022). Mongolia’s fossilised heritage. *Inner Asia*, 24, 131–161.
- Brusatte, S., Benson, R., Chure, D., Xu, X., Sullivan, C., & Hone, D. (2009). The first definitive carcharodontosaurid (Dinosauria: Theropoda) from Asia and the delayed ascent of tyrannosaurids. *Naturwissenschaften*, 96, 1051–1058.
- Brusatte, S., & Carr, T. (2016). The phylogeny and evolutionary history of tyrannosaurid dinosaurs. *Scientific Reports*, 6, 1–8.
- Brusatte, S., Carr, T., & Norell, M. (2012). The osteology of *Alioramus*, a gracile and long-snouted tyrannosaurid (Dinosauria: Theropoda) from the Late Cretaceous of Mongolia. *Bulletin of the American Museum of Natural History*, 366, 1–197.
- Brusatte, S. L., Norell, M. A., Carr, T. D., Erickson, G. M., Hutchinson, J. R., Balanoff, A. M., Bever, G. S., Choiniere, J. N., Makovicky, P. J., & Xu, X. (2010). Tyrannosaur paleobiology: New research on ancient exemplar organisms. *Science*, 329, 1481–1485.
- Carpenter, K. (1997). Evidence of predatory behavior by theropod dinosaurs. *Gaia*, 15, 135–144.
- Carpenter, K. (2002). Forelimb biomechanics of non-avian theropod dinosaurs in predation. *Senckenbergiana Lethaea*, 82, 59–76.
- Carr, T. D. (2020). A high-resolution growth series of *Tyrannosaurus rex* obtained from multiple lines of evidence. *PeerJ*, 8, 1–103.
- Chang, S.-C., Gao, K.-Q., Zhou, Z.-F., & Jourdan, F. (2017). New chronostratigraphic constraints on the Yixian formation with implications for the Jehol biota. *Palaeogeography, Palaeoclimatology, Palaeoecology*, 487, 399–406.
- Chin, K., Tokaryk, T., Erickson, G. M., & Calk, L. C. (1998). A king-size theropod coprolite. *Nature*, 393, 680–682.
- Coombs, W. P. (1978). Theoretical aspects of cursorial adaptations in dinosaurs. *The Quarterly Review of Biology*, 53, 393–418.
- Cost, I. N., Middleton, K. M., Sellers, K. C., Echols, M. S., Witmer, L. M., Davis, J. L., & Holliday, C. M. (2019). Palatal biomechanics and its significance for cranial kinesis in *Tyrannosaurus rex*. *The Anatomical Record*, 303, 999–1017.
- Currie, P. J. (1983). Hadrosaur trackways from the lower cretaceous of Canada. *Acta Palaeontologica Polonica*, 28, 63–73.
- Currie, P. J., & Eberth, D. (2010). On gregarious behavior in *Albertosaurus*. *Canadian Journal of Earth Sciences*, 47, 1277–1289.
- Dececchi, T. A., Mloszewski, A. M., Holtz, T. R., Jr., Habib, M. B., & Larsson, H. C. E. (2020). The fast and the frugal: Divergent locomotory strategies drive limb lengthening in theropod dinosaurs. *PLoS One*, 15, 1–24.
- DePalma, R. A., Burnham, D. A., Martin, L. D., Rothschild, B. M., & Larson, P. L. (2013). Physical evidence of predatory behavior in *Tyrannosaurus rex*. *Proceedings of the National Academy of Sciences*, 110, 12560–12564.
- Eberth, D. A. (1997). Judith River wedge. In P. J. Currie & K. Padian (Eds.), *Encyclopedia of dinosaurs* (pp. 199–204). Academic Press.
- Erickson, G. M., Makovicky, P. J., Currie, P. J., Norell, M. A., Yerby, S. A., & Brochu, C. A. (2004). Gigantism and comparative life history parameters of tyrannosaurid dinosaurs. *Nature*, 430, 772–775.
- Erickson, G. M., & Olson, K. H. (1996). Bite marks attributable to *Tyrannosaurus rex*: Preliminary description and implications. *Journal of Vertebrate Paleontology*, 16, 175–178.
- Ezcurra, M. D., Fiorelli, L. E., Martinelli, A. G., Rocher, S., von Baczko, M. B., Ezpeleta, M., Taborda, J. R. A., Hechenleitter, E. M., Trotteyn, M. J., & Desojo, J. B. (2017). Deep faunistic turnovers preceded the rise of dinosaurs in

- southwestern Pangaea. *Nature Ecology & Evolution*, 1, 1477–1483.
- Farlow, J. O. (1976). A consideration of the trophic dynamics of a Late Cretaceous large-dinosaur community (Oldman Formation). *Ecology*, 57, 841–857.
- Farlow, J. O., Brinkman, D. L., Abler, W. L., & Currie, P. J. (1991). Size, shape and serration density in theropod dinosaur lateral teeth. *Modern Geology*, 16, 161–198.
- Farlow, J. O., & Holtz, T. (2002). The fossil record of predation in dinosaurs. *The Paleontological Society Papers*, 8, 251–266.
- Farlow, J. O., & Pianka, E. R. (2002). Body size overlap, habitat partitioning and living space requirements of terrestrial vertebrate predators: Implications for the paleoecology of large theropod dinosaurs. *Historical Biology*, 16, 21–40.
- Foster, W., Brusatte, S., Carr, T., Williamson, T., Yi, L., & Lü, J. (2022). The cranial anatomy of the long-snouted tyrannosaurid dinosaur *Qianzhousaurus sinensis* from the upper cretaceous of China. *Journal of Vertebrate Paleontology*, 41, 1–30.
- Fowler, D. W., Woodward, H. N., Freedman, E. A., Larson, P. L., & Horner, J. R. (2011). Reanalysis of 'Raptor rex kriegsteini': A juvenile tyrannosaurid dinosaur from Mongolia. *PLoS One*, 6, 1–7.
- Gignac, P. M., & Erickson, G. M. (2016). Ontogenetic bite-force modeling of *Alligator mississippiensis*: Implications for dietary transitions in a large-bodied vertebrate and the evolution of crocodylian feeding. *Journal of Zoology*, 299, 229–238.
- Gignac, P. M., & Erickson, G. M. (2017). The biomechanics behind extreme osteophagy in *Tyrannosaurus rex*. *Scientific Reports*, 7, 1–10.
- Gignac, P. M., Makovicky, P., Erickson, G. M., & Walsh, R. (2010). A description of *Deinonychus antirrhopus* bite marks and estimates of bite force using tooth indentation simulations. *Journal of Vertebrate Paleontology*, 30, 1169–1177.
- Gignac, P. M., & O'Brien, H. (2016). Suchian feeding success at the interface of ontogeny and macroevolution. *Integrative and Comparative Biology*, 56, 449–458.
- Greaves, G. N., Greer, A. L., Lakes, R. S., & Rouxel, T. (2011). Poisson's ratio and modern materials. *Nature Materials*, 10, 823–837.
- Happ, J. (2008). An analysis of predator-prey behavior in a head-to-head encounter between *Tyrannosaurus rex* and *Triceratops*. In P. Larson & K. Carpenter (Eds.), *Tyrannosaurus rex: The tyrant king* (pp. 354–368). Indiana University Press.
- Holliday, C. M. (2009). New insights into dinosaur jaw muscle anatomy. *The Anatomical Record*, 292, 1246–1265.
- Holtz, T. (1994). The phylogenetic position of the Tyrannosauridae: Implications for theropod systematics. *Journal of Paleontology*, 68, 1100–1117.
- Holtz, T. (1995). The arctometatarsalian pes, an unusual structure of Cretaceous Theropoda (Dinosauria: Saurischia). *Journal of Vertebrate Paleontology*, 14, 480–519.
- Holtz, T. (2021). Theropod guild structure and the tyrannosaurid niche assimilation hypothesis: Implications for predatory dinosaur macroecology and ontogeny in later Late Cretaceous Asia-America. *Canadian Journal of Earth Sciences*, 58, 778–795.
- Hurum, J. H., & Sabath, K. (2003). Giant theropod dinosaurs from Asia and North America: Skulls of *Tarbosaurus bataar* and *Tyrannosaurus rex* compared. *Acta Palaeontologica Polonica*, 48, 161–190.
- Hutchinson, J. R., Bates, K. T., Molnar, J., Allen, V., & Makovicky, P. J. (2011). A computational analysis of limb and body dimensions in *Tyrannosaurus rex* with implications for locomotion, ontogeny, and growth. *PLoS One*, 6, e26037.
- Kundrát, M., Xu, X., Hančová, M., Gajdoš, A., Guo, Y., & Chen, D. (2018). Evolutionary disparity in the endoneurocranial configuration between small and gigantic tyrannosauroids. *Historical Biology*, 32, 1–15.
- Lautenschlager, S. (2013). Cranial myology and bite force performance of *Erlikosaurus andrewsi*: A novel approach for digital muscle reconstructions. *Journal of Anatomy*, 222, 260–272.
- Lü, J., Yi, L., Brusatte, S. L., Yang, L., Li, H., & Chen, L. (2014). A new clade of Asian Late Cretaceous long-snouted tyrannosauroids. *Nature Communications*, 5, 1–10.
- Maleev, E. A. (1955). Gigantic carnivorous dinosaurs from Mongolia. *Academy of Sciences USSR*, 104, 634–637.
- Maleev, E. A. (1974). Gigantic carnosauroids of the family Tyrannosauridae. *Trudy, Sovmestnaya Sovetskoye-Mongol'skaya Paleontologicheskaya Ekspeditsiya*, 1, 132–191.
- Marcé-Nogué, J., De Esteban-Trivigno, S., Püschel, T. A., & Fortuny, J. (2017). The intervals method: A new approach to analyse finite element outputs using multivariate statistics. *PeerJ*, 5, 1–21.
- Martinez, R., Sereno, P., Alcober, O., Colombi, C., Renne, P., Montañez, I., & Currie, B. (2011). A basal dinosaur from the dawn of the dinosaur era in southwestern Pangaea. *Science*, 331, 206–210.
- McCrea, R. T., Buckley, L. G., Farlow, J. O., Lockley, M. G., Currie, P. J., Matthews, N. A., & George Pemberton, S. (2014). A 'terror of tyrannosaurs': The first trackways of tyrannosauroids and evidence of gregariousness and pathology in tyrannosauridae. *PLoS One*, 9, 1–13.
- McKeown, M., Brusatte, S. L., Williamson, T. E., Schwab, J. A., Carr, T. D., Butler, I. B., Muir, A., Schroeder, K., Espy, M. A., Hunter, J. F., Losko, A. S., Nelson, R. O., Gautier, D. C., & Vogel, S. C. (2020). Neurosensory and sinus evolution as tyrannosauroid dinosaurs developed giant size: Insight from the endocranial anatomy of *Bistahieversor sealeyi*. *The Anatomical Record*, 303, 1043–1059.
- Molnar, R. E. (1991). The cranial morphology of *Tyrannosaurus rex*. *Palaeontographica Abteilung A*, 4–6, 137–176.
- Monteiro, L. R., & Soares, M. (1997). Allometric analysis of the ontogenetic variation and evolution of the skull in *Caiman spix*, 1825 (Crocodylia: Alligatoridae). *Herpetologica*, 53, 62–69.
- O'Brien, H., Lynch, L., Vliet, K., Brueggen, J., Erickson, G., & Gignac, P. (2019). Crocodylian head width allometry and phylogenetic prediction of body size in extinct crocodyliforms. *Integrative Organismal Biology*, 1, 1–15.
- Osborn, H. F. (1906). *Tyrannosaurus*, Upper Cretaceous carnivorous dinosaur (second communication). *Bulletin of the American Museum of Natural History*, 22, 281–296.
- Owocik, K., Kremer, B., Cotte, M., & Bocherens, H. (2019). Diet preferences and climate inferred from oxygen and carbon isotopes of tooth enamel of *Tarbosaurus bataar* (Nemegt Formation, Upper Cretaceous, Mongolia). *Palaeogeography, Palaeoclimatology, Palaeoecology*, 537, 1–16.
- Persons, W. S., & Currie, P. J. (2014). Duckbills on the run: The cursorial abilities of hadrosaurs and implications for tyrannosaur-avoidance strategies. In D. A. Eberth & D. C. Evans (Eds.), *Hadrosaurs* (pp. 449–458). Indiana University Press.
- Peterson, J. E., & Daus, K. N. (2019). Feeding traces attributable to juvenile *Tyrannosaurus rex* offer insight into ontogenetic dietary trends. *PeerJ*, 7, 1–17.



- Peterson, J. E., Tseng, Z. J., & Brink, S. (2021). Bite force estimates in juvenile *Tyrannosaurus rex* based on simulated puncture marks. *PeerJ*, 9, 1–18.
- Porro, L. B., Holliday, C. M., Anapol, F., Ontiveros, L. C., Ontiveros, L. T., & Ross, C. F. (2011). Free body analysis, beam mechanics, and finite element modeling of the mandible of *Alligator mississippiensis*. *Journal of Morphology*, 272, 910–937.
- Rahman, I. A., & Lautenschlager, S. (2016). Applications of three-dimensional box modeling to paleontological functional analysis. *The Paleontological Society Papers*, 22, 119–132.
- Rauhut, O., & Fechner, R. (2005). Early development of the facial region in a non-avian theropod dinosaur. *Proceedings of the Royal Society B: Biological Sciences*, 272, 1179–1183.
- Rauhut, O. W., Milner, A., & Moore-Fay, S. (2010). Cranial osteology and phylogenetic position of the theropod dinosaur *Proceratosaurus bradleyi* (Woodward, 1910) from the middle Jurassic of England. *Zoological Journal of the Linnean Society*, 158, 155–195.
- Rayfield, E. J. (2004). Cranial mechanics and feeding in *Tyrannosaurus rex*. *Proceedings of the Royal Society of London: Series Biological Sciences*, 271, 1451–1459.
- Rayfield, E. J. (2005a). Using finite-element analysis to investigate suture morphology: A case study using large carnivorous dinosaurs. *The Anatomical Record*, 283, 349–365.
- Rayfield, E. J. (2005b). Aspects of comparative cranial mechanics in the theropod dinosaurs *Coelophysis*, *Allosaurus* and *Tyrannosaurus*. *Zoological Journal of the Linnean Society*, 144, 309–316.
- Rayfield, E. J. (2007). Finite element analysis and understanding the biomechanics and evolution of living and fossil organisms. *Annual Review of Earth and Planetary Sciences*, 35, 541–576.
- Rothschild, B., & DePalma, R. (2013). Skin pathology in the cretaceous: Evidence for probable failed predation in a dinosaur. *Cretaceous Research*, 4, 44–47.
- Rowe, A., & Snively, E. (2021). Biomechanics of juvenile tyrannosaurid mandibles and their implications for bite force. *The Anatomical Record*, 10, 1–20.
- Rowe, A. J., & Rayfield, E. J. (2022). The efficacy of computed tomography scanning versus surface scanning in 3D finite element analysis. *PeerJ*, 10, 1–33.
- Russell, D. A. (1970). Tyrannosaurs from the Late Cretaceous of western Canada. *National Museum of Natural Sciences Publications in Paleontology*, 1, 1–34.
- Sakamoto, M. (2006). Scaling bite force in predatory animals: How does *T. Rex* compare with living predators? *Journal of Vertebrate Paleontology*, 26, 118A.
- Sakamoto, M. (2010). Jaw biomechanics and the evolution of biting performance in theropod dinosaurs. *Proceedings of the Royal Society B: Biological Sciences*, 277, 3327–3333.
- Schindelin, J., Arganda-Carreras, I., Frise, E., Kaynig, V., Longair, M., Pietzsch, T., Preibisch, S., Rueden, C., Saalfeld, S., Schmid, B., Tinevez, J. Y., White, D. J., Hartenstein, V., Eliceiri, K., Tomancak, P., & Cardona, A. (2012). Fiji: An open-source platform for biological-image analysis. *National Methods*, 9, 676–682.
- Schroeder, K., Lyons, S. K., & Smith, F. A. (2021). The influence of juvenile dinosaurs on community structure and diversity. *Science*, 371, 941–944.
- Snively, E., Henderson, D. M., & Phillips, D. S. (2006). Fused and vaulted nasals of tyrannosaurid dinosaurs: Implications for cranial strength and feeding mechanics. *Acta Palaeontologica Polonica*, 51, 435–454.
- Snively, E., O'Brien, H., Henderson, D. M., Mallison, H., Surring, L. A., Burns, M. E., Holtz, T. R., Jr., Russell, A. P., Witmer, L. M., Currie, P. J., Hartman, S. A., & Cotton, J. R. (2019). Lower rotational inertia and larger leg muscles indicate more rapid turns in tyrannosaurids than in other large theropods. *PeerJ*, 7, 1–43.
- Snively, E., Pennings, A., Johnson-Ransom, E. D., & Claxton, A. (2023). “Nutcracker” bite mechanics in *Tyrannosaurus rex* tested with multi-permutation structural analysis. *Journal of Vertebrate Paleontology* (SVP Book of Abstracts, accepted).
- Snively, E., & Russell, A. (2007). Functional variation of neck muscles and their relation to feeding style in Tyrannosauridae and other large theropod dinosaurs. *Anatomical Record*, 290, 934–957.
- Snively, E., & Russell, A. P. (2002). The Tyrannosaurid metatarsus: Bone strain and inferred ligament function. *Senckenbergiana Lethaea*, 82, 35–42.
- Snively, E., & Russell, A. P. (2003). A kinematic model of tyrannosaurid (Dinosauria, Theropoda) arctometatarsus function. *Journal of Morphology*, 255, 215–227.
- Snively, E., Russell, A. P., & Powell, G. L. (2004). Evolutionary morphology of the coelurosaurian arctometatarsus: Descriptive, morphometric, and phylogenetic approaches. *Zoological Journal of the Linnean Society*, 142, 525–553.
- Strait, D. S., Wang, Q., Dechow, P. C., Ross, C. F., Richmond, B. G., Spencer, M. A., & Patel, B. A. (2005). Modeling elastic properties in finite-element analysis: How much precision is needed to produce an accurate model? *The Anatomical Record Part A: Discoveries in Molecular, Cellular, and Evolutionary Biology*, 283, 275–287.
- Therrien, F., Henderson, D., & Ruff, C. (2005). Bite me – Biomechanical models of theropod mandibles and implications for feeding behavior. In K. Carpenter (Ed.), *The carnivorous dinosaurs* (pp. 179–230). Indiana University Press.
- Therrien, F., Zelenitsky, D. K., Voris, J. T., & Tanaka, K. (2021). Mandibular force profiles and tooth morphology in growth series of *Albertosaurus sarcophagus* and *Gorgosaurus libratus* (Tyrannosauridae: Albertosaurinae) provide evidence for an ontogenetic dietary shift in tyrannosaurids. *Canadian Journal of Earth Sciences*, 00, 1–17.
- Titus, A., Knoll, K., Sertich, J., Yamamura, D., Suarez, C., Glasspool, I., Ginouves, J., & Roberts, E. (2021). Geology and taphonomy of a unique tyrannosaurid bonebed from the upper Campanian Kaiparowits Formation of southern Utah: Implications for tyrannosaurid gregariousness. *PeerJ*, 9, 1–50.
- Tseng, Z. J. (2013). Testing adaptive hypotheses of convergence with functional landscapes: A case study of bone-cracking hypercarnivores. *PLoS One*, 8, 1–15.
- Tseng, Z. J., & Flynn, J. J. (2015). Are cranial biomechanical simulation data linked to known diets in extant taxa? A method for applying diet-biomechanics linkage models to infer feeding capability of extinct species. *PLoS One*, 10, 1–25.
- Tsuihiji, T., Watabe, M., Tsogtbaatar, K., Tsubamoto, T., Barsbold, R., Suzuki, S., Lee, A. H., Ridgely, R. C., Kawahara, Y., & Witmer, L. M. (2011). Cranial osteology of a



- juvenile specimen of *Tarbosaurus bataar* (Theropoda, Tyrannosauridae) from the Nemegt Formation (Upper Cretaceous) of Bugin Tsav, Mongolia. *Journal of Vertebrate Paleontology*, 31, 497–517.
- Varricchio, D. J. (2001). Gut contents from a cretaceous tyrannosaurid: Implications for theropod digestive tracts. *Journal of Paleontology*, 75, 401–406.
- Voris, J. T., Zelenitsky, D. K., Therrien, F., Ridgely, R. C., Currie, P. J., & Witmer, L. M. (2022). Two exceptionally preserved juvenile specimens of *Gorgosaurus libratus* (Tyrannosauridae, Albertosaurinae) provide new insight into the timing of ontogenetic changes in tyrannosaurids. *Journal of Vertebrate Paleontology*, 41, 1–21.
- Whiteside, J. H., Olsen, P. E., Eglinton, T., Brookfield, M. E., & Sambrotto, R. N. (2010). Compound-specific carbon isotopes from Earth's largest flood basalt eruptions directly linked to the end-Triassic mass extinction. *PNAS*, 107, 6721–6725.
- Witmer, L. M. (1995). The extant phylogenetic bracket and the importance of reconstructing soft tissues in fossils. In J. J. Thomason (Ed.), *Functional morphology in vertebrate paleontology* (Vol. 1, pp. 19–33). Cambridge University Press.
- Woodward, H. N., Tremaine, K., Williams, S. A., Zanno, L. E., Horner, J. R., & Myrhvold, N. (2020). Growing up *Tyrannosaurus rex*: Osteohistology refutes the pygmy “*Nanotyrannus*” and supports ontogenetic niche partitioning in juvenile *Tyrannosaurus*. *Science Advances*, 6, 1–8.
- Xing, L., Bell, P. R., Currie, P. J., Shibata, M., Tseng, K., & Dong, Z. (2012). A sauropod rib with an embedded theropod tooth: Direct evidence for feeding behaviour in the Jehol group, China. *Lethaia*, 01, 1–7.
- Xu, X., Clark, J., Forster, C., Norell, M., Erickson, G. M., Eberth, D., Jia, C., & Zhao, Q. (2006). A basal tyrannosauroid dinosaur from the Late Jurassic of China. *Nature*, 439, 715–718.
- Xu, X., Norell, M. A., Kuang, X., Wang, X., Zhao, Q., & Jia, C. (2004). Basal tyrannosauroids from China and evidence for protofeathers in tyrannosauroids. *Nature*, 431, 680–684.
- Xu, X., Wang, K., Zhang, K., Ma, Q., Xing, L., Sullivan, C., Hu, D., Cheng, S., & Wang, S. (2012). A gigantic feathered dinosaur from the lower cretaceous of China. *Nature*, 484, 92–95.
- Zanno, L. E., & Makovicky, P. J. (2013). Neovenatorid theropods are apex predators in the Late Cretaceous of North America. *Nature Communications*, 4, 1–9.
- Zanno, L. E., & Sampson, S. D. (2005). A new oviraptorosaur (Theropoda; Maniraptora) from the Late Cretaceous (Campanian) of Utah. *Journal of Vertebrate Paleontology*, 25, 897–904.
- Zanno, L. E., Tucker, R. T., Canoville, A., Avrahami, H. M., Gates, T. A., & Makovicky, P. J. (2019). Diminutive fleet-footed tyrannosauroid narrows the 70-million-year gap in the North American fossil record. *Communications Biology*, 2, 1–12.
- Zatsiorsky, V., & Prilutsky, B. (2012). *Biomechanics of skeletal muscles*. Human Kinetics.
- Zhou, Z. (2006). Evolutionary radiation of the Jehol biota: Chronological and ecological perspectives. *Geological Journal*, 41, 377–393.

## SUPPORTING INFORMATION

Additional supporting information can be found online in the Supporting Information section at the end of this article.

**How to cite this article:** Johnson-Ransom, E., Li, F., Xu, X., Ramos, R., Midzuk, A. J., Thon, U., Atkins-Weltman, K., & Snively, E. (2023). Comparative cranial biomechanics reveal that Late Cretaceous tyrannosaurids exerted relatively greater bite force than in early-diverging tyrannosauroids. *The Anatomical Record*, 1–21. <https://doi.org/10.1002/ar.25326>